THE JOURNAL OF BIOLOGICAL CHEMISTRY VOL. 283, NO. 44, pp. 30273–30288, October 31, 2008

15-Deoxy-Δ(12,14)-prostaglandin J_2 Induces Vascular Endothelial Cell Apoptosis through the Sequential Activation of MAPKS and p53*[S]

Received for publication, June 2, 2008, and in revised form, August 7, 2008 Published, JBC Papers in Press, August 21, 2008, DOI 10.1074/jbc.M804196200

Tsung-Chuan Ho[‡], Show-Li Chen[§], Yuh-Cheng Yang[‡¶‖], Chia-Yi Chen[‡], Fang-Ping Feng[‡], Jui-Wen Hsieh[¶], Huey-Chuan Cheng[**], and Yeou-Ping Tsao[‡**‡‡1]**

*From the Departments of [‡]Medical Research and **Ophthalmology, Mackay Memorial Hospital, the [§]Department of Microbiology, School of Medicine, National Taiwan University, the [¶]Mackay Medicine, Nursing and Management College, the [‖]School of Medicine, Taipei Medical University, and the [‡‡]Department of Microbiology and Immunology, The National Defense Medical Center, Taipei 251, Taiwan*

15-Deoxy-Δ(12,14)-prostaglandin J_2 (15d-PGJ_2) is a potent anti-angiogenic factor and induces endothelial cell apoptosis, although the mechanism remains unclear. In this study, 15d-PGJ_2 was found to increase p53 levels of the human umbilical vein endothelial cells by stabilizing p53. Both 15d-PGJ_2-induced apoptosis and the induction of $p21^{Waf1}$ and Bax can be abolished by p53 small interfering RNA but not by peroxisome proliferator-activated receptor γ inhibitors. Moreover, 15d-PGJ_2 activated JNK and p38 MAPK while inducing p53 phosphorylation at sites responsible for p53 activity. JNK inhibitor (SP600125) or p38 MAPK inhibitor (SB203580) pretreatment attenuated 15d-PGJ_2-mediated apoptosis and suppressed the $p21^{Waf1}$ and Bax expressions without affecting p53 protein accumulation. Pretreatment with SP600125 partially prevented the phosphorylation of p53 at serines 33 and 392 induced by 15d-PGJ_2. 15d-PGJ_2 was also found to induce reactive oxygen species generation and partially blocked nuclear factor-κB activity. Pretreatment with antioxidant *N*-acetylcysteine prevented the p53 accumulation, the phosphorylations of JNK and p38 MAPK, the inhibition of NF-κB activity, as well as the apoptosis induced by 15d-PGJ_2. Using a mouse model of corneal neovascularization, it was demonstrated *in vivo* that 15d-PGJ_2 induced reactive oxygen species generation, activated JNK and p38 MAPK, induced p53 accumulation/phosphorylation, and induced vascular endothelial cell apoptosis, which could be abolished by *N*-acetylcysteine, SP600125, SB203580, or a virus-derived amphipathic peptides-based p53 small interfering RNA. This is the first study that 15d-PGJ_2 induces vascular endothelial cell apoptosis through the signaling of JNK and p38 MAPK-mediated p53 activation both *in vitro* and *in vivo*, further establishing the potential of 15d-PGJ_2 as an anti-angiogenesis agent.

Neovascularization is involved in important pathological processes such as age-related macular degeneration, arthritis, and solid tumor growth. Hypoxia and inflammation-mediated vascular endothelial cell growth factor (VEGF)[2] induction is generally accepted as the driving force of new vessel growth (1). Angiogenesis is thus a target of therapy, and there is an active search for agents capable of arresting both new vessel growth *in vivo* and the proliferation of vessel endothelial cells (EC) *in vitro*. Among these agents is 15-deoxy-Δ(12,14)-prostaglandin J_2 (15d-PGJ_2). 15d-PGJ_2 has been reported to act as an anti-angiogenic factor by inducing EC apoptosis (2–7) and suppressing angiogenic factor-induced EC proliferation, tube-like differentiation, and VEGF receptor expression (2, 3). An earlier study reported that the rat corneal neovascularization induced by VEGF can be significantly suppressed by co-implanted 15d-PGJ_2 (3). Interestingly, it remains unclear whether 15d-PGJ_2 can suppress the progression of existing neovessels. In this regard, the apoptotic-inducing capacity of 15d-PGJ_2 *in vivo* is also unclear.

15d-PGJ_2 is a member of the cyclopentenone prostaglandins and is synthesized in many cell types in response to extrinsic stimuli (8). 15d-PGJ_2 is an end product of the cyclooxygenase pathways, in which 15d-PGJ_2 is produced by dehydration of prostaglandin D_2 (9). In contrast to other prostaglandins that have specific transmembrane receptors, no specific 15d-PGJ_2 cell surface receptor has been identified to date. 15d-PGJ_2 has been shown to act through direct interactions with its intracellular targets; for example, it is known to be a ligand of the nuclear transcriptional factor peroxisome proliferator-activated receptor γ (PPARγ) (10, 11). PPARγ binding to 15d-PGJ_2 allows translocation from the cytoplasm into the nucleus to regulate a variety of genes involved in cell differentiation, lipid biosynthesis, glucose metabolism, immune response, and vas-

* This work was supported by Grants NSC 95-2314-B-195-009-MY3 and NSC 96-3112-B-195-001 from the National Science Council, Taiwan, and Grant MMH-E-96006 from Mackay Memorial Hospital. The costs of publication of this article were defrayed in part by the payment of page charges. This article must therefore be hereby marked "*advertisement*" in accordance with 18 U.S.C. Section 1734 solely to indicate this fact.

[S] The on-line version of this article (available at http://www.jbc.org) contains supplemental Fig. S1.

[1] To whom correspondence should be addressed. Tel.: 886-2-28094661, ext. 3076; Fax: 886-2-28085952; E-mail: yptsao@yahoo.com.

[2] The abbreviations used are: VEGF, vascular endothelial cell growth factor; 15d-PGJ_2, 15-deoxy-Δ(12,14)-prostaglandin J_2; HUVEC, human umbilical vein endothelial cells; MAPK, mitogen-activated protein kinase; JNK, c-Jun NH_2-terminal kinase; PPARγ, peroxisome proliferator-activated receptor γ; PEDF, pigment epithelium-derived factor; siRNA, small interfering RNA; NF-κB, nuclear factor-κB; ROS, reactive oxygen species; H2DCFDA, 2′,7′-dichlorodihydrofluorescein diacetate; NAC, *N*-acetylcysteine; FITC, fluorescein isothiocyanate; EC, endothelial cell; CGZ, ciglitazone; TGZ, troglitazone; DCF, 2′,7′-dichlorofluorescein; RT, reverse transcriptase; PBS, phosphate-buffered saline; eNOS, endothelial nitric-oxide synthase.

culature (12, 13). Notably, the cyclopentenone moiety of 15d-PGJ_2 contains an electrophilic carbon that can react covalently with nucleophiles such as the free sulfhydryls of GSH and cysteine residues in cellular proteins (14). Most PPARγ ligands lack the electrophilic cyclopentenone. 15d-PGJ_2 thus induces some PPARγ-independent biological actions through its electrophilic activity, such as inhibition of nuclear factor-κB (NF-κB) signaling through covalent modifications of critical cysteine residues in IκB kinase and the DNA-binding domains of NF-κB subunits (15).

The induction of apoptosis in proliferating ECs is an available strategy in the treatment of diseases relative to neovascularization. The mechanism of 15d-PGJ_2 induction of EC apoptosis has been suggested to be through the activation of PPARγ (2, 6). Interestingly, our recent study on pigment epithelium-derived factor (PEDF) identified the sequential activation of PPARγ and p53 as a signaling mechanism of EC apoptosis (16). PPARγ is thus a potential mechanism for 15d-PGJ_2-induced apoptosis. However, a recent study indicates that 15d-PGJ_2-induced HUVEC apoptosis is PPARγ-independent (7). The PPARγ-independent effect is also supported by evidence that the cyclopentenone ring alone can dose-dependently induce HUVEC apoptosis (5). In addition, several pro-apoptotic signals induced by 15d-PGJ_2 have been shown to be independent of PPARγ in cell types other than ECs. These include accumulation of the p53 tumor suppressor protein in SH-SY5Y human neuroblastoma cells (17) and the activation of p38 mitogen-activated protein kinase (MAPK) in human articular chondrocytes (18) and in a human pancreatic cancer cell line (19). Based on this conflicting information, the involvement of PPARγ remains to be clarified. Unlike PPARγ, the involvement of p53 in EC apoptosis induced by 15d-PGJ_2 is more plausible. p53 is a well established pro-apoptotic protein. p53 is involved in the apoptosis or cell cycle arrest of ECs induced by PEDF (16), adenovirus-mediated *p53* gene transfer (20), and paclitaxel (Taxol) (21). Moreover, p53 protein expression is induced by 15d-PGJ_2 (6, 17). However, the necessity of p53 in 15d-PGJ_2-induced EC apoptosis has never been established.

MAPKs, including stress-activated c-Jun NH_2-terminal kinase (JNK), p38 MAPK, and extracellular signal-regulated kinase (ERK), have been found to respond to a variety of extracellular stimuli and to determine cell fate under stress (22, 23). Emerging evidence indicates that 15d-PGJ_2 can activate MAPKs in ECs. For example, 15d-PGJ_2 can enhance DNA binding of AP-1 by inducing c-Jun phosphorylation via JNK activation (4, 24). 15d-PGJ_2 has also been shown to activate p38 MAPK in ECV304 cells (6). However, the potential involvement of these kinases in the EC apoptosis induced by 15d-PGJ_2 has not been established. Here we demonstrate that 15d-PGJ_2 induces apoptosis of HUVECs and ECs in chemical burn-induced vessels on mouse cornea through the signaling of p53 and that p53 activation is achieved by JNK and p38 MAPK-mediated modulation of p53 phosphorylation.

EXPERIMENTAL PROCEDURES

Cell Culture and Treatment—HUVECs (Cascade Biologics, Inc., Portland, OR) were grown in Medium 200 with Low Serum Growth Supplement (LSGS kit, supplement contains 1.9% fetal bovine serum, 3 ng/ml basic fibroblast growth factor, 10 μg/ml heparin, 1 μg/ml hydrocortisone, and 10 ng/ml epidermal growth factor). Culture plates were coated with 2% gelatin. Cells (passages 4–8) were cultured at 37 °C in a humidified atmosphere of 5% CO_2. To prepare 15d-PGJ_2 (Cayman Chemical, Ann Arbor, MI), the original solvent methyl acetate was evaporated under a gentle stream of nitrogen, and then it was redissolved in PBS before adding to the medium. Treatments with 15d-PGJ_2 (10 μM, unless specified), recombinant PEDF derived from *Escherichia coli* (25), MAPKs inhibitors, PPARγ antagonists, NF-κB inhibitors (Calbiochem), or NAC (Sigma) were performed 4 h after seeding (5×10^5 cells/well of 6-well plate) in LSGS medium.

Animals and Treatment—BALB/c mice, weighing 25–35 g, were anesthetized with injections of ketamine. An alkaline burn was created by touching the cornea for 20 s with a 3-mm-diameter disk containing 1 N NaOH. The ocular surface was then irrigated with 20 ml of physiological saline. At 3 days after the injury, the mice were randomly divided into the 15d-PGJ_2 treatment group and control group, with 10 mice per group. For treatment, 20 μl of 20 μM 15d-PGJ_2 or 15d-PGJ_2 in combination with 80 μM MAPKs inhibitors was dropped onto the cornea, two times at an interval of 4 h. For NAC treatment, corneas were covered with 20 μl of 10 mM NAC for 30 min, before treatment with 15d-PGJ_2. The control group received 20 μl of saline eye drops. For evaluation of apoptosis, the corneas were treated twice at an interval of 4 h, and corneas were harvested 24 h after the second treatment. At the end of the treatment, corneas with iris intact were dissected from the eyes for evaluation of ROS generation or apoptosis without fixation. Corneas designated for immunofluorescent assay were first fixed with 4% paraformaldehyde for 2 h. All animal experiments were conducted in accordance with the Association for Research in Vision and Ophthalmology Statement for the Use of Animals in Ophthalmic and Vision Research.

Evaluation of Apoptosis—The percentage of HUVEC apoptosis was calculated using TACS annexin V-FITC kit (R & D Systems, Minneapolis, MN). Stained cells were analyzed by flow cytometry (FACSCalibur; Beckman) as described previously (16). The percentage of annexin V-positive cells was also confirmed by *in situ* staining according to the manufacturer's instruction. The cell number was monitored by counterstaining with Hoechst 33342. The nuclei were calculated in 10 randomly selected fields of the three different chambers (~7200 cells). Specimens were examined and photographed on a Zeiss epifluorescence microscope (×40, 10 fields/sample). Pictures were recorded on Zeiss software.

To determine whether 15d-PGJ_2 has any apoptotic effect on vascular ECs, the corneas were incubated with 10% goat serum and 1% bovine serum albumin for 30 min at 4 °C and then double-labeled with annexin V-FITC (R & D Systems) and PECAM-1 (1:200 dilution, Santa Cruz Biotechnology, Santa Cruz, CA) for 1 h at room temperature. Following labeling, the cornea was washed twice in PBS and fixed with 4% paraformaldehyde for 20 min. The cornea was incubated with rhodamine-conjugated goat anti-mouse IgG antibody (1:500 dilution; Santa Cruz Biotechnology) for 1 h at room temperature, and cell nuclei were monitored by counterstaining with Hoechst 33342

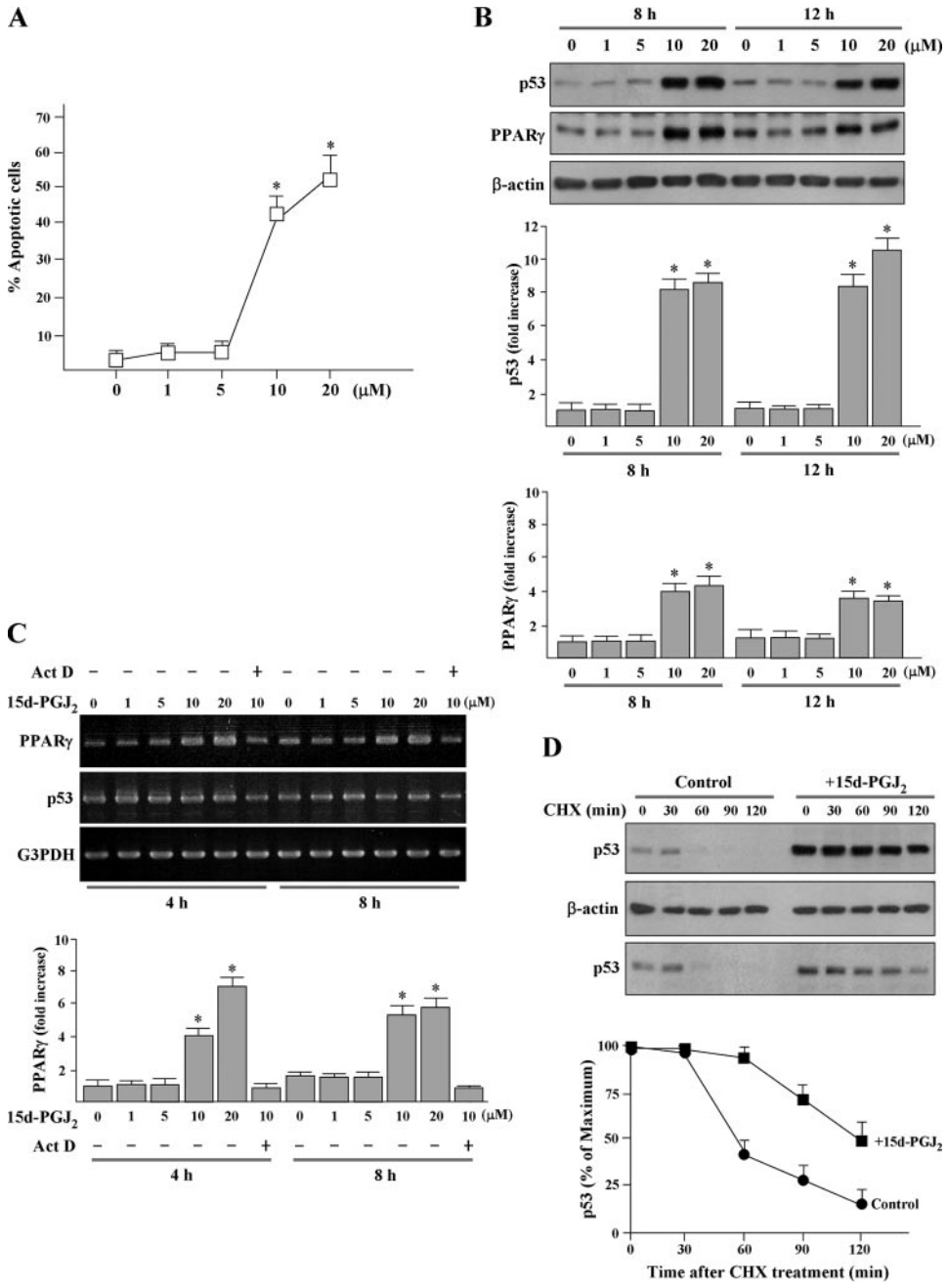

FIGURE 1. **15d-PGJ$_2$ induces apoptosis and increases protein levels of p53 and PPARγ in HUVECs.** *A*, effects of 15d-PGJ$_2$ on cell apoptosis at different concentrations. Cells were exposed to 1–20 μM 15d-PGJ$_2$ for 16 h. Apoptotic cell number was determined using the annexin V-FITC apoptosis detection kit. Stained cells were analyzed by flow cytometry. *, $p < 0.05$ *versus* untreated cells. *B*, 15d-PGJ$_2$ dose-dependently causes elevation of p53 and PPARγ protein levels. HUVECs were treated with 15d-PGJ$_2$ (1–20 μM) for the indicated time periods, and p53 and PPARγ were detected by Western blot analysis. Representative blots (*top panels*) and densitometric analysis with S.D. (*bottom figures*) are shown. *, $p < 0.02$ *versus* untreated cells. *C*, HUVECs were pretreated with 10 ng/ml actinomycin D (*ActD*) for 3 h, and then incubated with 15d-PGJ$_2$ for the indicated time periods. Total RNA was extracted, and RT-PCR analysis for p53 and PPARγ were performed. Glyceraldehyde-3-phosphate dehydrogenase (*G3PDH*) expression was examined for normalization purposes. The results are representative of three independent experiments. *, $p < 0.05$ *versus* untreated cells. *D*, 15d-PGJ$_2$ stimulation increases the stability of endogenous p53. HUVECs were stimulated with 15d-PGJ$_2$ or left untreated (control) for 8 h. All cultures were then treated with 20 μM cycloheximide (*CHX*) for the times indicated. The total p53 level from cell extracts was detected using Western blotting with an anti-p53 antibody. The levels of p53 were estimated based on the intensity of p53 bands at different time points shown in the *upper panel* and normalized to β-actin. Blot 3 shows p53 image obtained from 4 μg of cell extracts of 15d-PGJ$_2$-treated cells compared with 20 μg of cell extracts of untreated cells.

for 2 min. After final washes and mounting, apoptotic cells were counted in randomly selected fields using a Leica confocal microscope (×40, 10 fields/cornea).

Western Blot Analysis—Cells were scraped into lysis buffer (150 μl/35-mm well) containing 20 mM HEPES (pH 7.4), 1% SDS, 150 mM NaCl, 1 mM EGTA, 5 mM β-glycerophosphate, 10 μg/ml leupeptin, and 10 μg/ml aprotinin. Samples containing 20 μg of protein were analyzed by SDS-PAGE and then were electrotransferred to polyvinylidene difluoride membranes (Immobilon-P; Millipore, Bedford, MA) and processed for immunoblot analysis. Antibodies used in this study were for active p38 MAPK and active JNK (Promega, Madison, WI), p38 MAPK/SAPK2, JNK (Upstate Biotechnology, Lake Placid, NY), p53 (Chemicon, Temecula, CA), phospho-p53, phospho-NF-κB, p65 (Ser-536), c-Jun, ATF2, NF-κB, p65, phospho-IκB-α (Ser-32/36), IκB-α (Cell Signaling Technology, Beverley, MA), cleaved caspase-3 (Abcam Ltd., Cambridge, UK), and β-actin (Sigma). Proteins of interest were detected using the appropriate IgG-horseradish peroxidase secondary antibody (Santa Cruz Biotechnology) and ECL reagent (Amersham Biosciences). X-ray films were scanned on the model GS-700 Imaging Densitometer (Bio-Rad) and analyzed using Labworks 4.0 software. For quantification, blots of at least three independent experiments were used.

p53 Small Interfering RNA Treatment—Human and mouse p53 and control siRNAs were purchased from Santa Cruz Biotechnology. For the transfection procedure, HUVECs were grown to 70% confluence, and siRNA was transfected using INTERFERin siRNA transfection reagent (PolyPlus-Transfection, San Marcos, CA) according to the manufacturer's instructions. The final concentration of siRNA was 10 nM. By 8 h after siRNA transfection, HUVECs were resuspended in new culture media with recovery for 36 h and then treated with 15d-PGJ$_2$.

Transfection of p53 siRNA into endothelial cell on mouse cornea was achieved by using the DeliverX Plus siRNA transfection kit (Panomics, Fremont, CA), a virus-derived amphipathic peptides-based kit following

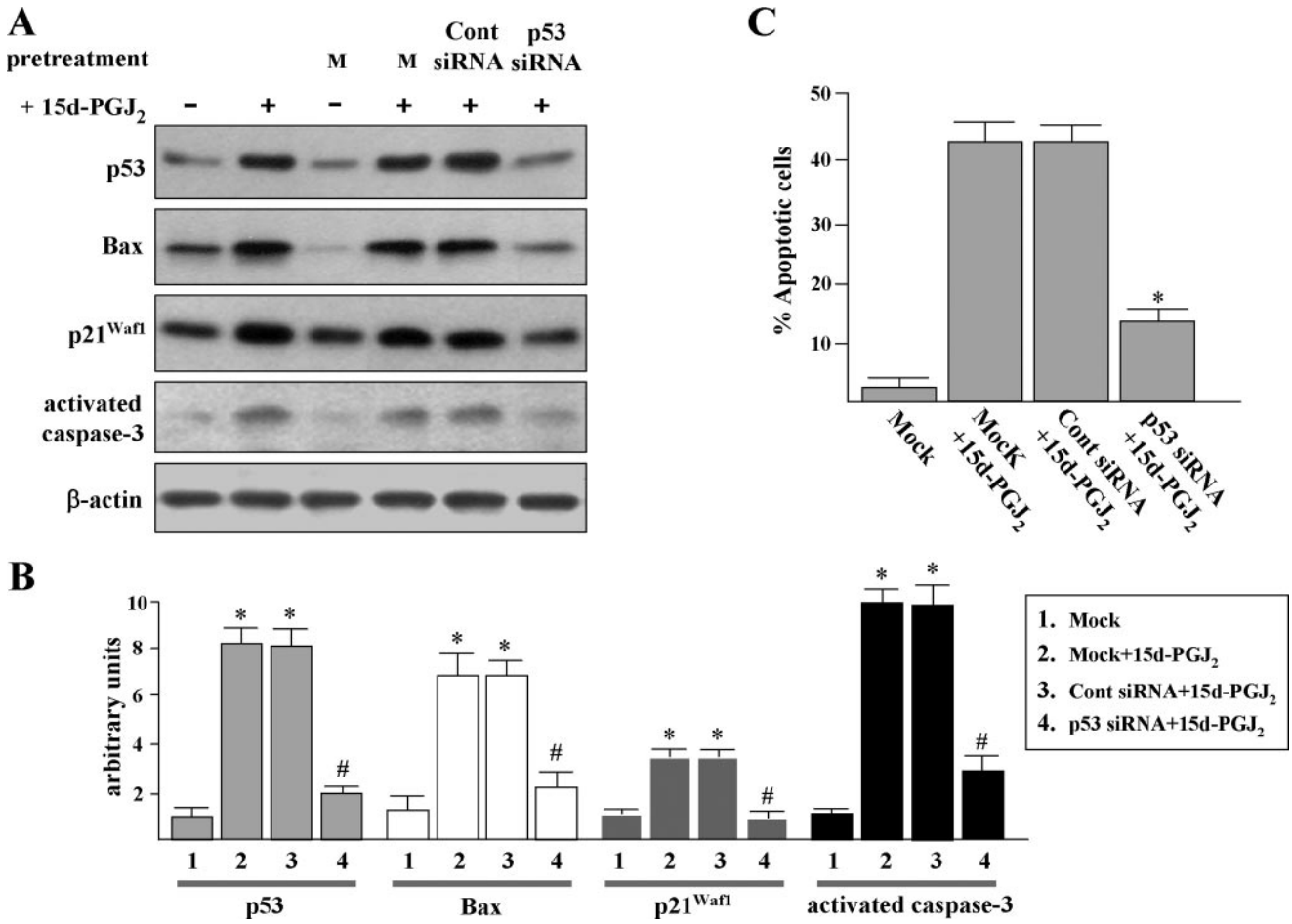

FIGURE 2. **p53 siRNA suppresses the 15d-PGJ$_2$-induced Bax and p21^{Waf1} expression and procaspase-3 cleavage and reduces the 15d-PGJ$_2$-induced HUVEC apoptosis.** *A,* HUVECs were transfected with p53 siRNA or control siRNA for 8 h and allowed to recover for a further 36 h. Cells were treated with 15d-PGJ$_2$ for an additional 10 h, and cell lysate was then isolated for Western blot analysis of p53, Bax, and p21^{Waf1}. Parts of the 15d-PGJ$_2$-treated cells were harvested after treatment for 16 h for detecting the cleaved caspase-3 (17 kDa). "Mock (*M*)" indicates that cells were treated with transfection reagent. *B,* densitometric analysis of *A*. *, $p < 0.02$ *versus* mock-treated cells. #, $p < 0.05$ *versus* control siRNA-pretreated cells. *C,* apoptosis was quantified by using the annexin V-FITC apoptosis detection kit. *, $p < 0.05$ *versus* control siRNA-pretreated cells.

the manufacturer's instruction. Briefly, 5 μmol/liter working stock of mouse p53 siRNA or control siRNA was mixed with sonicated transfection reagent and incubated at 37 °C for 20 min to generate the working siRNA transfection complex. The final concentration of siRNA was 100 nM. Next, each mouse cornea was eye-dropped with 20 μl of sonicated siRNA transfection reagent alone (mock control) or siRNA transfection complex twice at an interval of 4 h, and recovery was for a further 24 h before 15d-PGJ$_2$ treatment. The transfection efficiency was determined, in separated experiments, using a FITC-labeled nonsilencing control siRNA (Santa Cruz Biotechnology). Results revealed that almost all of vascular ECs and epithelial cells of cornea can be transfected and still maintain normal morphologies. No green fluorescence can be detected without using the transfection reagent.

Semi-quantitative Reverse Transcriptase (RT)-PCR—Total RNA was extracted from HUVECs with TRIzol reagent (Invitrogen). Synthesis of cDNA was performed with 1 μg of total RNA at 50 °C for 50 min, using oligo(dT) primers and reverse transcriptase (Superscript III, Invitrogen). The amplification mixture (final volume, 20 μl) contained 1× *Taq* polymerase buffer, 0.2 mM dNTPs, 1.5 mM $MgCl_2$, 1 μM primer pair, and 0.5 unit of *Taq*DNA polymerase (Invitrogen). cDNA was equalized in an 18–26 cycle amplification reaction with PPARγ primers 5′-CAGGAGCAGAGCAAAGAGGTG-3′ (forward)/5′-CAAACTCAAACTTGGGCTCCA-3′ (reverse) or p53 primers 5′-GCGCACAGAGGAAGAGAATC-3′ (forward)/5′-TGAGTCAGGCCCTTCTGTCT-3′ (reverse) yielding 300- and 330-bp products, respectively. The number of cycles for the primer sets (denaturation, 30 s, 94 °C; annealing, 30 s, 61 °C; and polymerization, 30 s, 72 °C) was chosen to be in the linear range of amplification. The PCR products were subjected to electrophoresis on 2% agarose gel, and the DNA was visualized by staining with ethidium bromide under ultraviolet irradiation. The intensities of the PCR products were quantified by densitometrically using a FUJI LAS-3000 system and multigauge version 1.01 software (FUJIFILM, Tokyo, Japan).

Immunofluorescent—Mouse corneas were treated at 4 °C with methanol for 2 min and blocked with 10% goat serum and 5% bovine serum albumin for 1 h at room temperature. Corneas were stained with antibodies to monoclonal anti-mouse eNOS antibody (1:200; Pharmingen), active p38 MAPK or active JNK (1:500; Promega), or phospho-p53 (1:500; Cell Signaling Technology), or p53 (1:500, ab4060; Abcam Ltd.), or NF-κB p65

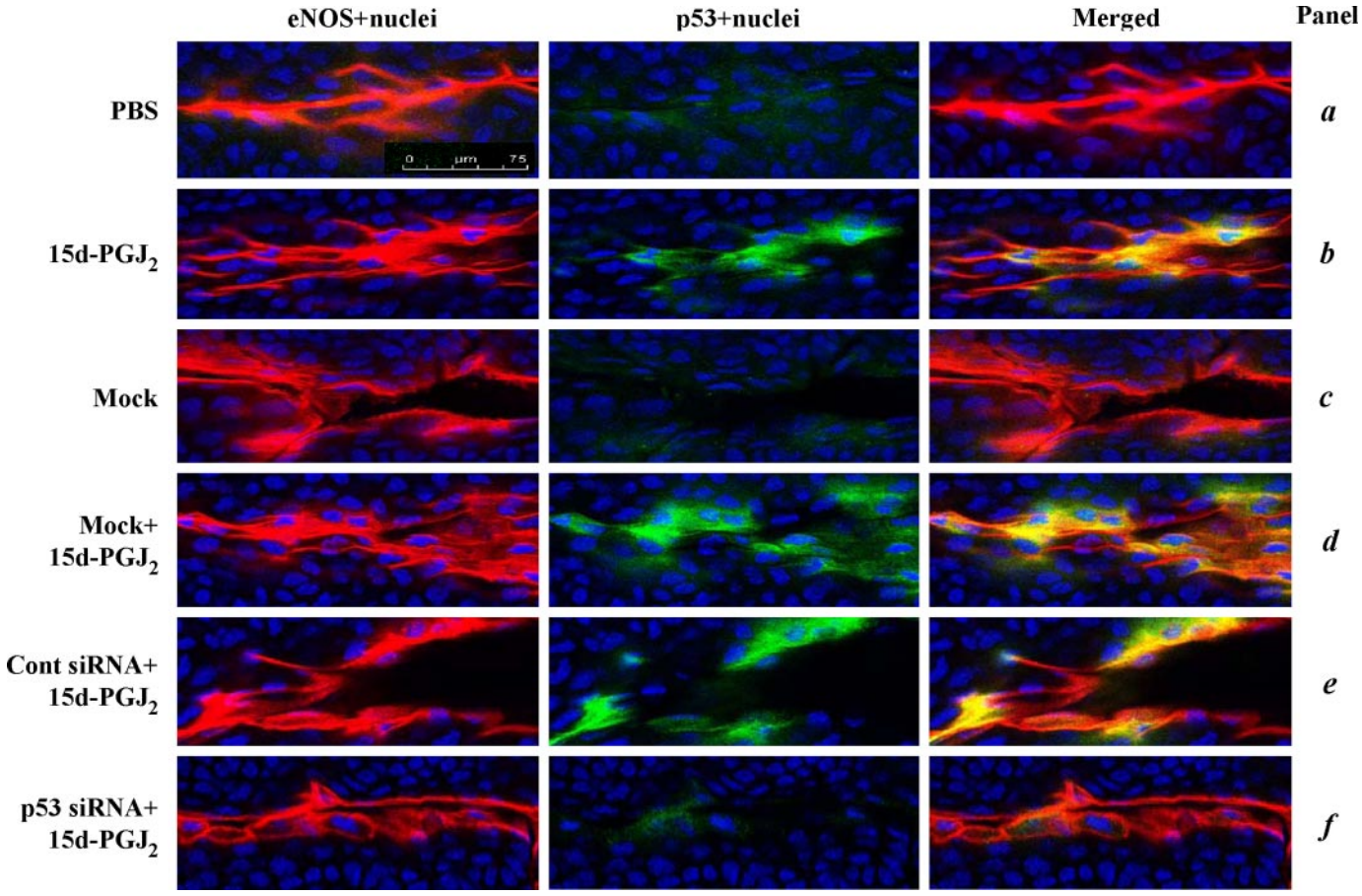

FIGURE 3. **15d-PGJ$_2$ induces p53 protein expression in vascular ECs.** Mouse corneas were subjected to alkali trauma and at 3 days later treated with either mock transfection reagent (virus-derived amphipathic peptide alone), control siRNA, or p53 siRNA transfection mixture. After recovery for a further 24 h, the corneas were treated with PBS or 20 μM 15d-PGJ$_2$ for a further 8 h. The corneas were then harvested and subjected to immunofluorescence for eNOS (*red*; specific for vascular endothelium) and p53 (*green*). Nuclei were stained by Hoechst 33342 (*blue*). p53 localized in the nucleus (*pale blue*) and co-localized with the eNOS (*yellow*) is shown in merged images. Representative data from experiments are shown. Magnification, ×40. *Bar,* 75 μm.

(1:500; Cell Signaling Technology) at 4 °C overnight, followed by incubation with both rhodamine-conjugated goat anti-mouse IgG antibody and FITC-conjugated goat anti-rabbit IgG antibody (1:500; Santa Cruz Biotechnology) for 1 h at room temperature. Nuclei were located by counterstaining with Hoechst 33342 for 20 min. After final washes and mounting, corneas were examined using a Leica confocal microscope (×40). p-p53 (Ser-392)-positive cells were counted in randomly selected fields (×40, 10 fields/cornea).

Detection of ROS by H$_2$DCFDA—The intracellular ROS generation was assayed using 2′,7′-dichlorodihydrofluorescein diacetate (H$_2$DCFDA), and when oxidized by ROS it releases the green fluorescent compound 2′,7′-dichlorofluorescein (DCF).

(i) To detect ROS by spectrofluorometric assay, 1.2 × 10^4 cells were seeded in a 2% gelatin-coated 96-well plate and incubated for a further 4 h. After 15d-PGJ$_2$ treatment, cells were washed with PBS (pH 7.4) and then incubated with fresh medium containing 5 μM H$_2$DCFDA (Molecular Probes, Eugene, OR) in the dark for 15 min at 37 °C. Fluorescence (excitation, 488 nm; emission, 520 nm) was measured with a SpectraMAX GEMINI Reader (Molecular Devices, Sunnyvale, CA). The background fluorescence from control wells without the addition of H$_2$DCFDA was subtracted from experimental readings.

(ii) For monitoring the DCF fluorescence in HUVECs, cells were plated on 2% gelatin-coated plate in LSGS medium. After 15d-PGJ$_2$ treatment and H$_2$DCFDA exposure as described above, cells were washed two times with LSGS medium and fixed with 4% paraformaldehyde for 15 min. Nuclei were stained with Hoechst 33342. Fluorescence images were taken with an inverted fluorescence microscope (Olympus Optical Co., Ltd., Melville, NY).

(iii) For detection of ROS in vascular ECs, after 15d-PGJ$_2$ treatment for 1 h, corneas were dissected from animal eyes and transferred into a 12-well plate. Individual cornea was then incubated with 1 ml of LSGS medium containing 5 μM H$_2$DCFDA for 20 min at 37 °C and then washed two times with LSGS medium. Corneas were then fixed with 4% paraformaldehyde for 15 min and stained with Hoechst 33342. Fluorescence images were taken with a Leica confocal microscope (10 fields/cornea).

Determination of NF-κB Activation—NF-κB p50/p65 transcription factor colorimetric assay (SGT510, Chemicon International, Temecula, CA) was used to measure the active NF-κB in nuclear extracts by following the manufacturer's instruc-

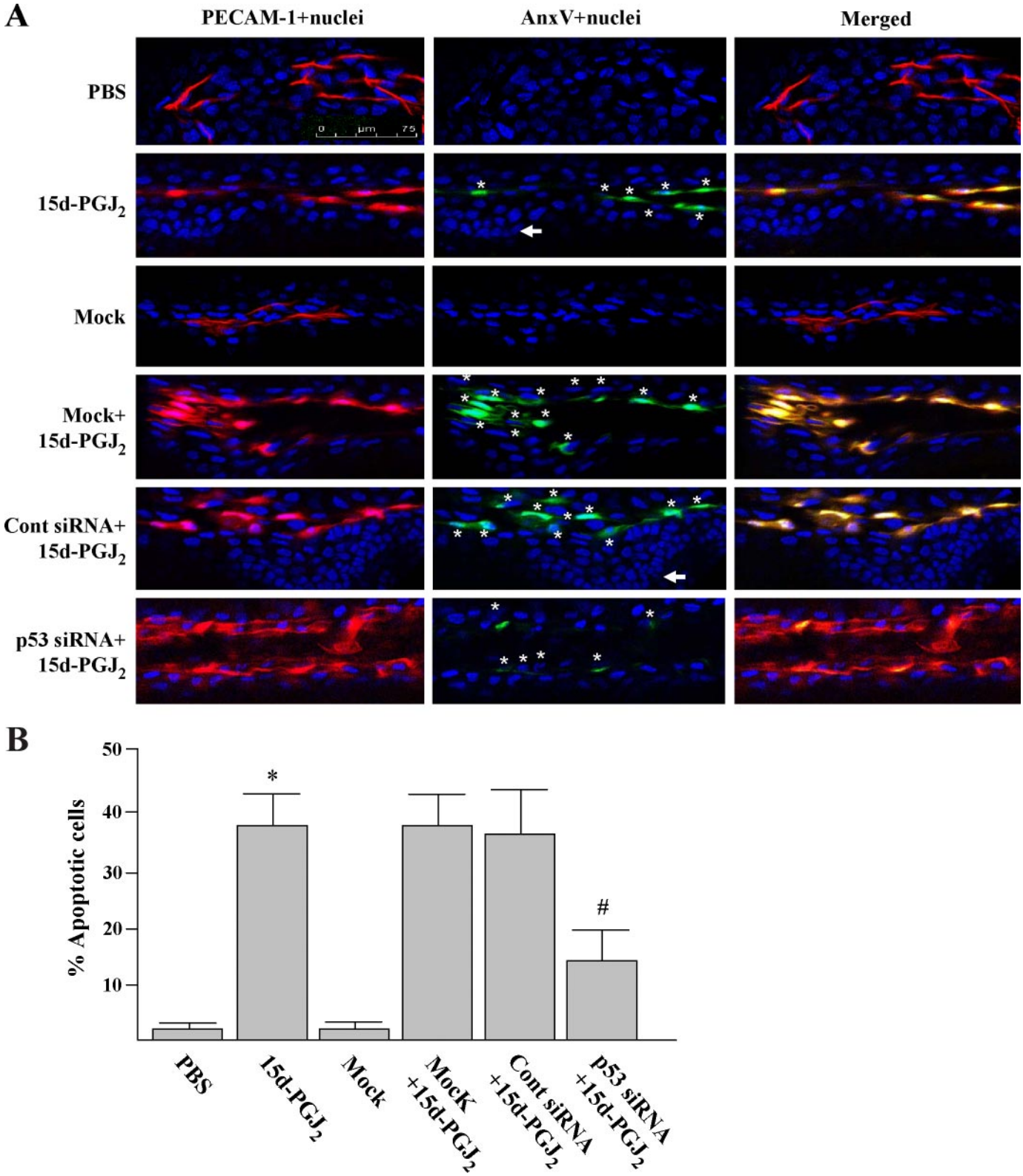

FIGURE 4. **p53 siRNA represses the 15d-PGJ_2-induced vascular EC apoptosis.** Animal treatment is described under "Experimental Procedures." After treatment for 24 h, corneas were harvested and double-stained with annexin V-FITC (apoptotic cells in *green*) and PECAM-1 (EC in *red*). Nuclei were stained by Hoechst 33342 (*blue*). Magnification, ×40. Apoptotic ECs (nuclei surrounded by annexin V; marked with a *star*, and *yellow*) were detected by superimposing two images using a digital imaging program. *A,* representative images from three independent experiments. *Arrows* indicate a nucleus with typical nuclear morphology of corneal epithelial cells. *B,* percentages of annexin V-positive ECs were quantified under a microscope (×40, 10 fields/cornea). *, $p < 0.05$ *versus* PBS-treated corneas; #, $p < 0.05$ *versus* control siRNA-pretreated corneas.

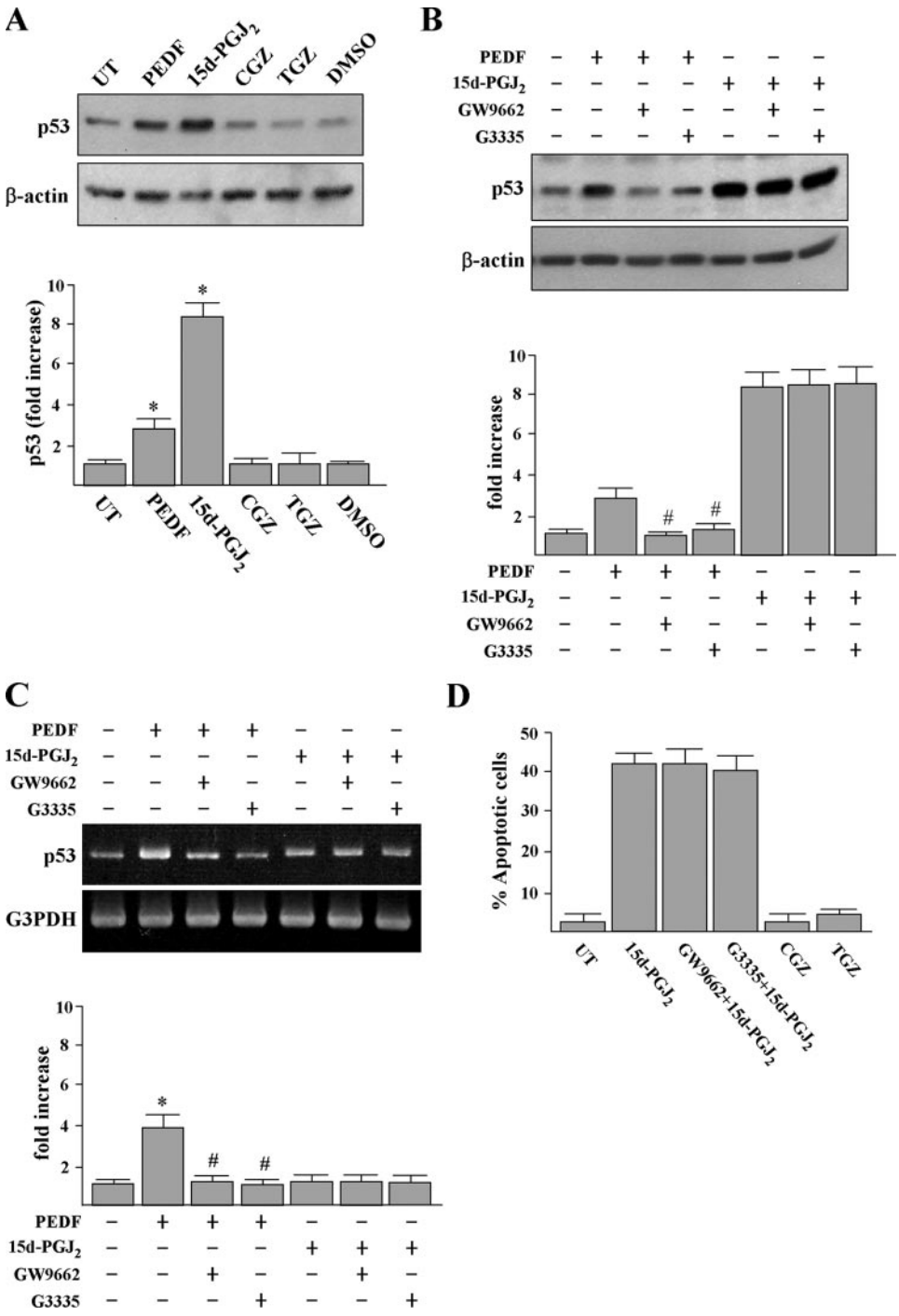

FIGURE 5. **PPARγ agonist and antagonist effects on p53 expression and apoptosis in HUVECs.** *A,* cells were treated with 200 ng/ml PEDF or 10 μM PPARγ agonists (15d-PGJ_2, CGZ, and TGZ) or DMSO solvent for 12 h, and p53 protein was detected by Western blot analysis. *, $p < 0.05$ *versus* untreated (*UT*) cells. *B* and *C,* HUVECs were pretreated with 10 μM PPARγ antagonists (GW9662 and G3335) for 1 h prior to incubation with PEDF or 15d-PGJ_2 for an additional 10 h. Cellular proteins and total RNA were then extracted for Western blot analysis and RT-PCR analysis. Representative blots (*top panels*) and densitometric analysis with S.D. (*bottom figure*) are shown. *, $p < 0.05$ *versus* untreated cells. #, $p < 0.001$ *versus* PEDF-treated cells. *D,* apoptosis was quantified by using the annexin V-FITC apoptosis detection kit.

tions. Briefly, nuclear extracts from 5×10^5 HUVECs were prepared using the NE-PER nuclear and cytoplasmic extraction kit (Pierce). Double-stranded biotinylated oligonucleotides containing the consensus sequence for NF-κB binding (5′-GGGACTTTCC-3′) were mixed with nuclear extract and assay buffer. After incubation, the mixture was transferred to the streptavidin-coated ELISA kit processed following the manufacturer's instruction and read at 450 nm using a SpectraMAX GEMINI Reader (Molecular Devices). For each experiment, triplicate samples were measured for statistical significance. The specificity of binding was confirmed by competition with unlabeled oligonucleotides.

Statistical Analyses—Data are expressed as means ± S.D. of three to five independent experiments. The Mann-Whitney *U* test was used to determine statistically significant differences. p values <0.05 were considered significant.

RESULTS

15d-PGJ_2 Dose-dependently Induces Apoptosis and Increases Protein Levels of p53 and PPARγ—Exposure of HUVECs to 10 μM or greater 15d-PGJ_2 for 16 h increased the percentage of annexin V-positive apoptotic cells to 40% (Fig. 1*A*). Using 10 μM or greater 15d-PGJ_2 markedly induced PPARγ and p53 protein accumulation at all time periods studied (Fig. 1*B*). RT-PCR showed that the levels of p53 mRNA were similar to untreated cells at all time periods studied, suggesting that transcription of p53 is not activated (Fig. 1*C*). Because the half-life of p53 protein is short in most primary cells, further experiments were performed to investigate whether 15d-PGJ_2 can enhance the protein stability of p53 and showed that 15d-PGJ_2 prolonged the half-life of p53 in HUVECs (Fig. 1*D*). On the other hand, the level of PPARγ mRNA was increased at 4–8 h, as compared with control (Fig. 1*C*). Pretreatment with actinomycin D for 3 h prior to 15d-PGJ_2 exposure suppressed the PPARγ mRNA level, suggesting that the increase of PPARγ mRNA is transcription-dependent.

p53 Is Critical for 15d-PGJ_2-mediated Apoptosis of HUVECs and Vascular ECs on Mouse Cornea—To investigate whether p53 protein is required for 15d-PGJ_2-mediated apoptosis, HUVECs were transfected with p53-specific siRNA before 15d-PGJ_2 treatment. Western blotting verified that the p53 induction was specifically and significantly reduced by the cognate p53 siRNA (Fig. 2, *A* and *B*). Impor-

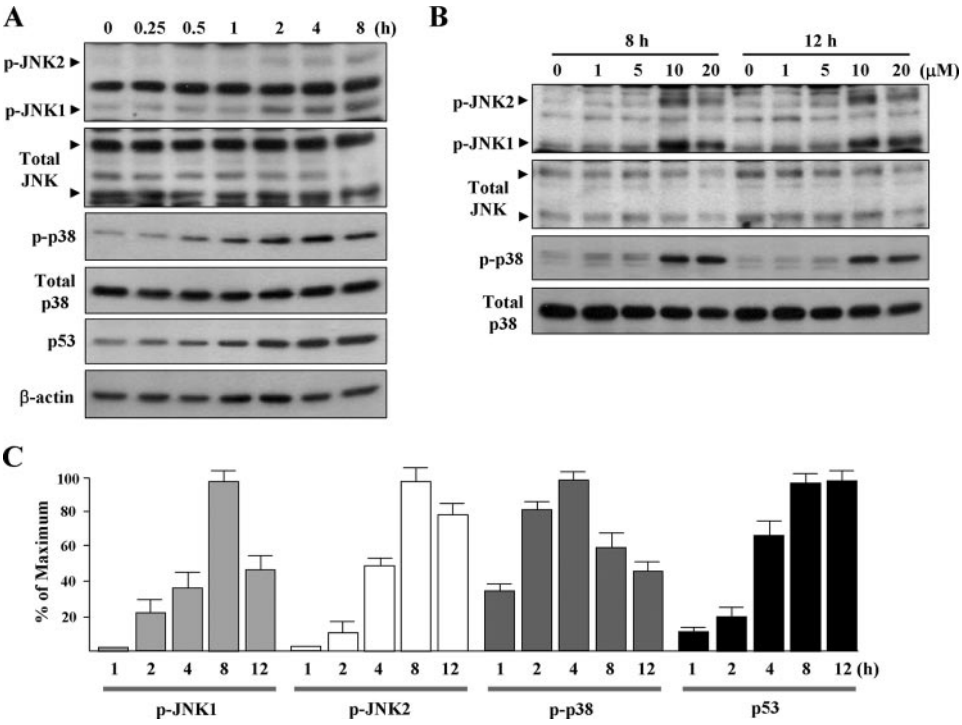

FIGURE 6. **15d-PGJ$_2$ dose- and time-dependently induces JNK and p38 MAPK phosphorylation.** *A*, HUVECs were exposed to 15d-PGJ$_2$ for the indicated time periods. Western blotting was performed to detect the active phosphorylated forms of JNK (*p-JNK*) and p38 MAPK (*p-p38*) and is shown in the *upper panels*. Antibodies were then stripped and re-incubated with anti-JNK and anti-p38 MAPK antibodies (*lower panels*), respectively, to detect the levels of total JNK and p38 MAPK. *B,* HUVECs were exposed to 1–20 μM of 15d-PGJ$_2$ for the times indicated. Western blotting was performed as described above. *C,* intensities of p-JNK1/2, p-p38 MAPK, and p53 were determined by densitometry.

tantly, compared with either mock or control siRNA transfections, p53 siRNA significantly reduced 15d-PGJ$_2$-induced apoptosis (Fig. 2*C*) as well as Bax and p21^{Waf1} expressions and procaspase-3 cleavages (Fig. 2*B*).

To determine whether 15d-PGJ$_2$ can also increase p53 protein *in vivo*, we investigated the ECs in abnormal vessels induced by alkali burn on mouse corneas. As shown in Fig. 3, immunofluorescent assay showed that there is a base-line p53 (*green*) in both vascular ECs and epithelial cells of cornea. The identity of ECs was confirmed by an endothelial cell antigen (eNOS; Fig. 3, *red*). Treatment of cornea with 15d-PGJ$_2$ for 8 h specifically enhanced p53 protein in the vascular ECs but not in the corneal epithelium (Fig. 3, *panel b*). The induced p53 was localized at both of the cytoplasms as the distribution of eNOS (Fig. 3, *yellow*) and the nucleus (*pale blue*).

To verify if 15d-PGJ$_2$ can induce EC apoptosis *in vivo*, we examined the EC apoptosis by staining corneas with an endothelial cell surface marker (PECAM-1; Fig. 4*A*, *red*) and an apoptotic-specific agent (annexin V; *green*). We found that 15d-PGJ$_2$ treatment for 24 h induced a greater number of apoptotic loci (*yellow*) in the vascular ECs as compared with saline treatment (Fig. 4*A*). The PECAM-1/annexin V double staining also revealed that cornea epithelium (PECAM-1 negative) was completely insensitive to 15d-PGJ$_2$ treatment (Fig. 4*A,* indicated by *arrow*), indicating the specific induction of EC apoptosis by 15d-PGJ$_2$.

To investigate whether p53 protein is required for 15d-PGJ$_2$-mediated apoptosis *in vivo*, the cornea was transfected with mouse p53-specific siRNA by a virus-based transfection reagent before 15d-PGJ$_2$ treatment. Immunofluorescent assay verified that the p53 induction was specifically and significantly reduced by the cognate p53 siRNA. Control siRNA pretreatment had no such inhibitory effect (Fig. 3, *panel f* compared with *panels d* and *e*). We also noted that mouse p53-specific siRNA pretreatment caused further decrease of the basal level of p53 in corneal epithelium. Importantly, compared with either mock or control siRNA transfections, p53 siRNA pretreatment significantly reduced 15d-PGJ$_2$-induced apoptosis (Fig. 4*B*; 13.4 ± 6% *versus* 37.5 ± 7%). These results indicate that 15d-PGJ$_2$ can induce p53 protein expression in vascular ECs/ and the p53 protein plays a critical role in 15d-PGJ$_2$-mediated EC apoptosis *in vivo*.

p53 Protein Accumulation and Apoptosis Induced by 15d-PGJ$_2$ Are Independent of PPARγ Activation—Because 15d-PGJ$_2$ is one of the natural ligands of PPARγ, we further examined the involvement of PPARγ in p53 protein accumulation. First, we tested whether PEDF, a protein that induces p53 through PPARγ (16) or other PPARγ agonists, troglitazone (TGZ) and ciglitazone (CGZ), can cause p53 protein accumulation. Incubation of HUVECs with PEDF or 10 μM PPARγ agonists for 12 h revealed that the levels of p53 were increased by PEDF and 15d-PGJ$_2$ but not by TGZ or CGZ (Fig. 5*A*). Treatment of HUVECs with TGZ or CGZ at up to 20 μM also did not increase p53.[3] Second, PPARγ antagonists GW9662 or G3335 had no apparent inhibitory effect on 15d-PGJ$_2$-induced p53 accumulation although, as expected, GW9662 or G3335 can markedly inhibit PEDF-induced p53 expression at both mRNA and protein levels (Fig. 5, *B* and *C*). 15d-PGJ$_2$-induced HUVEC apoptosis was not blocked by GW9662 or G3335 pretreatment (Fig. 5*D*). In control experiments, TGZ and CGZ had no effect on induction of HUVEC apoptosis. The GW9662 pretreatment could significantly prevent PEDF-induced HUVEC apoptosis (data not shown). Taken together, our results indicate that 15d-PGJ$_2$ induces apoptosis and p53 accumulation through a PPARγ-independent mechanism.

15d-PGJ$_2$ Induces Phosphorylations of JNK and p38 MAPK—We further investigated whether 15d-PGJ$_2$ affects JNK and p38 MAPK signaling in HUVECs by Western blot analysis using antibodies against the active phosphorylated forms of JNK and

[3] T.-C. Ho and Y.-P. Tsao, unpublished results.

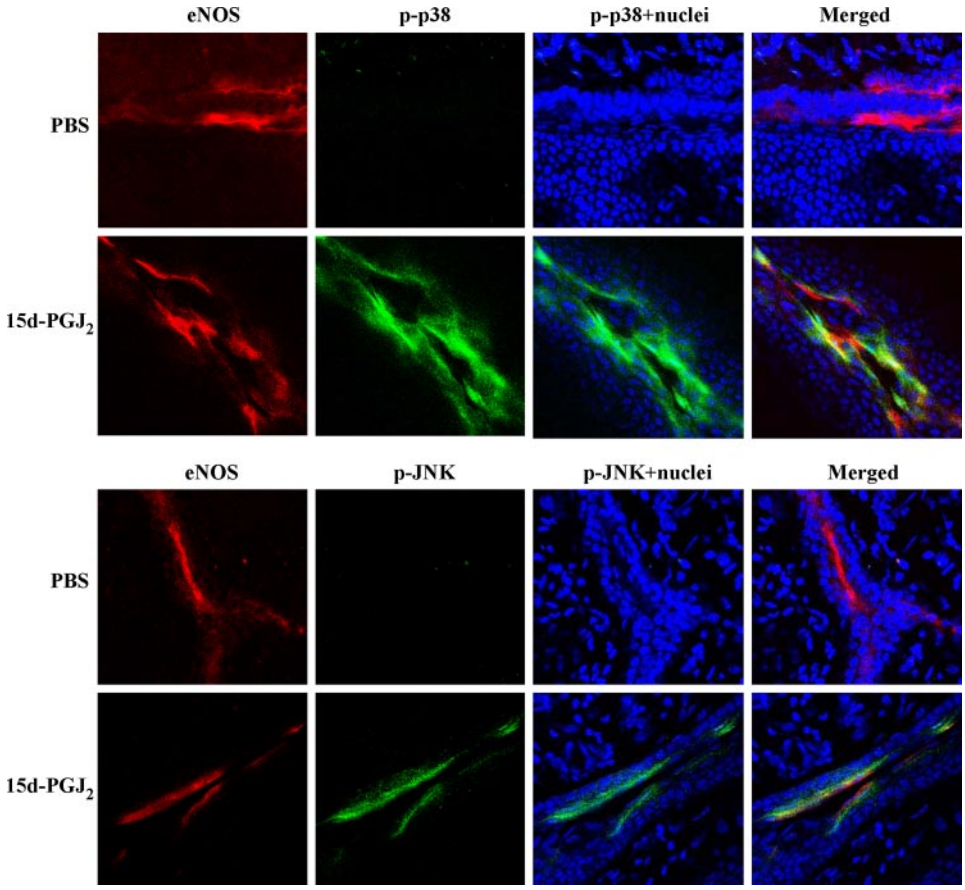

FIGURE 7. **15d-PGJ$_2$ induces JNK and p38 MAPK phosphorylation in vascular ECs.** Mouse corneas were subjected to alkali trauma and treated 3 days later with either 20 μl of PBS or 20 μM 15d-PGJ$_2$. After treatment for 8 h, corneas were harvested and subjected to immunofluorescent assay for eNOS (*red*; specific for vascular endothelium) and p-JNK or p-p38 MAPK (*green*). Nuclei were stained by Hoechst 33342 (*blue*). p-JNK and p-p38 MAPK localized in the nuclei (*pale blue*) and co-localized with eNOS (*yellow*) are shown in merged images. Magnification ×40. *Bar,* 75 μm.

p38 MAPK. Results revealed that JNK1/2 and p38 MAPK were phosphorylated after 15d-PGJ$_2$ treatment for 1–2 h. The peak phosphorylation of JNK1/2 and p38 MAPK occurred 4–8 h after treatment (Fig. 6, *A* and *C*); phosphorylation was sustained for up to 12 h (Fig. 6*B*). 15d-PGJ$_2$ also induced p53 accumulation in a time-dependent manner (Fig. 6, *A* and *C*). In addition, similar to apoptosis and p53 accumulation, phosphorylations of JNK and p38 MAPK only respond to 10 μM or higher concentrations of 15d-PGJ$_2$ (Fig. 6*B*).

To determine whether 15d-PGJ$_2$ can also induce phosphorylations of JNK and p38 MAPK *in vivo*, we investigated the ECs in abnormal vessels induced by alkali burn on mouse corneas. Immunofluorescent assay showed that nearly every cell that stained positively for eNOS (*red*) also stained positively for p-JNK or p-p38 MAPK (Fig. 7, *yellow*) when the corneas were exposed to 15d-PGJ$_2$ for 8 h. In addition, a portion of the induced p-JNK and p-p38 MAPK was translocated to the nucleus (Fig. 7, *pale blue*), a feature of JNK or p38 MAPK activation. Saline had no effect on JNK and p38 MAPK phosphorylation and translocation. We also noted that 15d-PGJ$_2$ does not induce phosphorylations of JNK and p38 MAPK in the corneal epithelium and the eNOS negative cells. Thus, 15d-PGJ$_2$ stimulates the activation of JNK and p38 MAPK in vascular ECs *in vivo*.

Inhibition of JNK and p38 MAPK Silences p53-induced Bax and p21^{Waf1} Expression and Partially Prevents p53-induced Apoptosis—We then examined whether JNK or p38 MAPK activation is involved in the p53 protein accumulation induced by 15d-PGJ$_2$. Western blotting results revealed that the induced p53 levels could not be prevented by cells pretreated with a JNK inhibitor (5–10 μM SP600125) or a p38 MAPK inhibitor (5–10 μM SB203580) (Fig. 8*A* and Fig. 9*A*), indicating that JNK and p38 MAPK are not responsible for p53 accumulation. On the other hand, p53-induced Bax and p21^{Waf1} were completely attenuated by SP600125 or SB203580 pretreatments (Fig. 8*A*).

The efficacy and specificity of p38 MAPK and JNK inhibitors are evident from the Western blot analysis of the phosphorylation levels of ATF2, a documented substrate of p38 MAPK, and c-Jun, a documented substrate of JNK. As shown in Fig. 8*A*, 15d-PGJ$_2$ stimulation caused ATF2 and c-Jun phosphorylation. Importantly, the phosphorylated c-Jun level was not significantly affected by SB203580, and phosphorylated ATF2 level was not affected by SP600125.

Above all, the involvement of JNK and p38 MAPK in the signaling of 15d-PGJ$_2$-induced HUVEC apoptosis was established by the observation that pretreatment with SP600125 or SB203580 (10 μM, 1 h) prevented 15d-PGJ$_2$-induced HUVEC apoptosis from 42 ± 4% to 13 ± 5 and 11 ± 2%, respectively (Fig. 8*B*). In control experiments, 10 μM of SP600125 or SB203580 was not cytotoxic to HUVECs. Pretreatment with combined SP600125 and SB203580 had no further cytoprotective effect against 15d-PGJ$_2$ stimulation. Taken together, our results revealed that the apoptosis and expressions of Bax and p21^{Waf1} induced by 15d-PGJ$_2$ was mediated by JNK and p38 MAPK activation.

To confirm the effect of MAPK inhibitors on 15d-PGJ$_2$-induced apoptosis *in vivo*, we examined the EC apoptosis induced by 15d-PGJ$_2$ by staining corneas with an endothelial cell marker (PECAM-1) and an apoptotic-specific agent (annexin V). We found that either SP600125 or SB203580 treatment could significantly reduced the 15d-PGJ$_2$-induced apoptosis from 37.5 ± 6% to 7 ± 4 and 7 ± 5%, respectively (Fig. 8*C*). Treatment with saline, SP600125, or SB203580 alone did not induce EC apoptosis. These findings suggest that JNK and p38 MAPK are participating in 15d-PGJ$_2$-induced apoptosis of vascular ECs on mouse cornea.

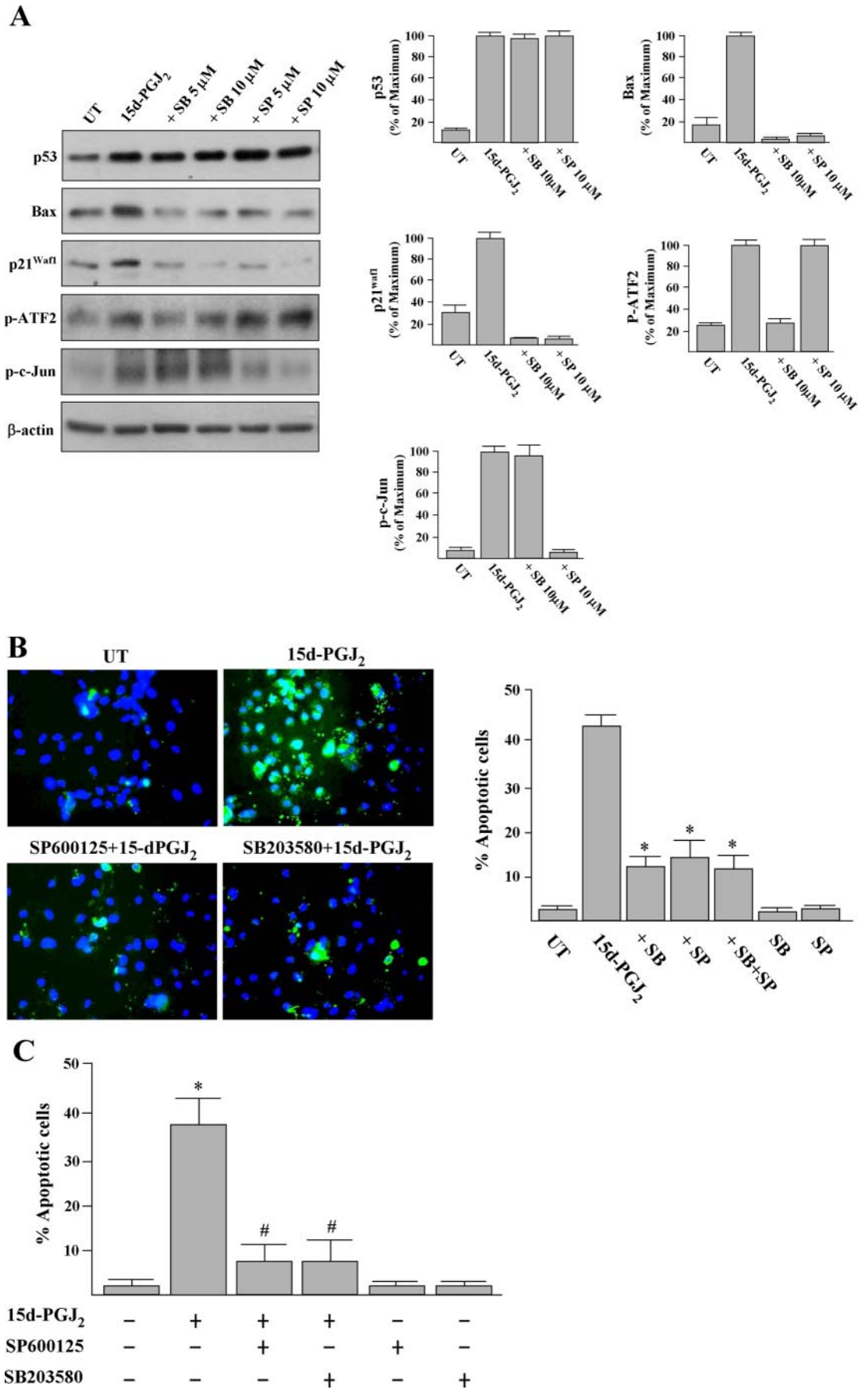
A
UT
15d-PGJ2
+SB 5 μM
+SB 10 μM
+SP 5 μM
+SP 10 μM
p53
Bax
p21Waf1
p-ATF2
p-c-Jun
β-actin
p53 (% of Maximum)
Bax (% of Maximum)
p21waf1 (% of Maximum)
P-ATF2 (% of Maximum)
p-c-Jun (% of Maximum)
+SB 10μM
+SP 10 μM
B
UT
15d-PGJ2
SP600125+15-dPGJ2
SB203580+15d-PGJ2
% Apoptotic cells
+SB
+SP
+SB+SP
SB
SP
C
% Apoptotic cells
15d-PGJ2
SP600125
SB203580

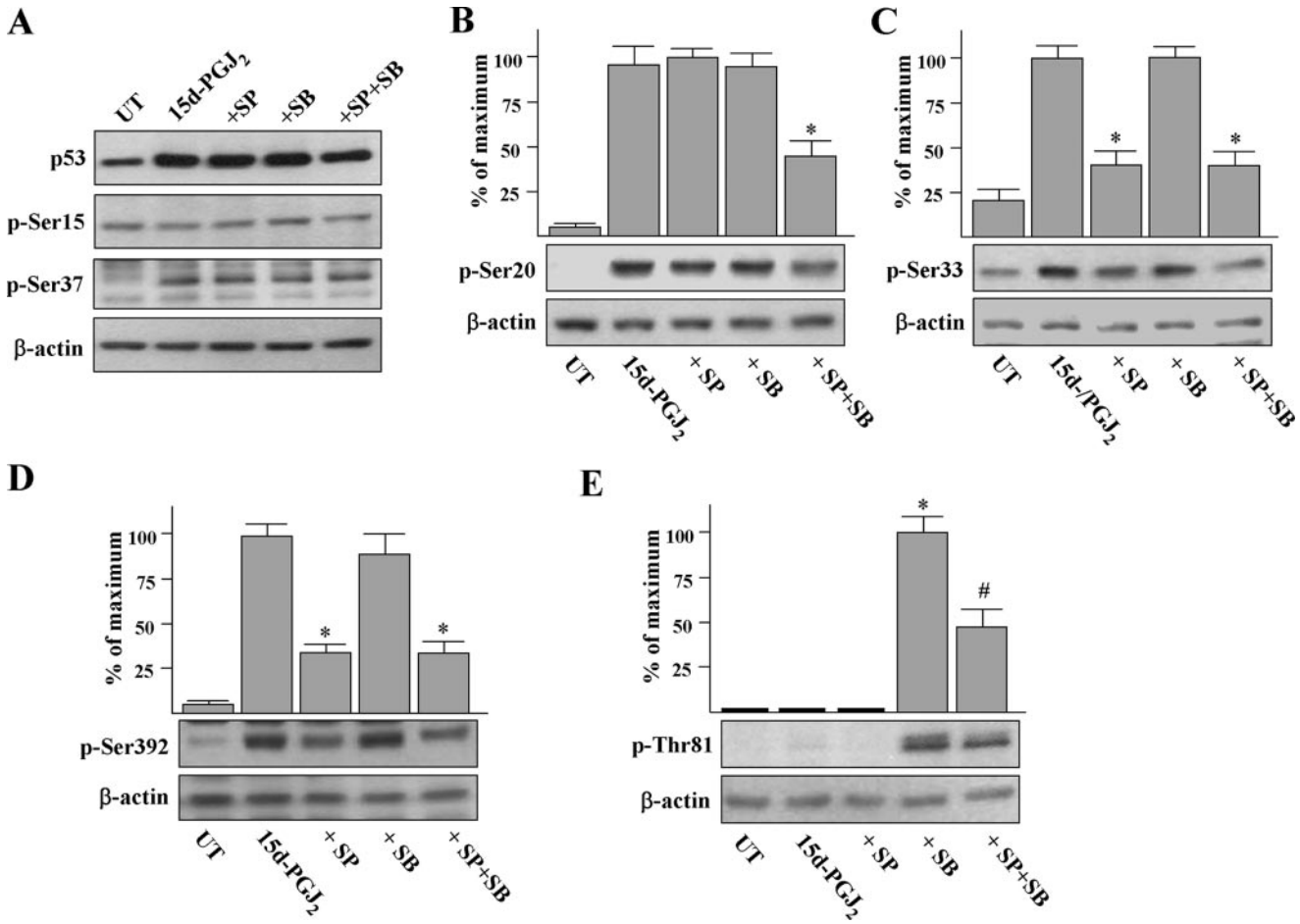

FIGURE 9. **The effects of MAPK inhibitors SP600125 (*SP*) and SB203580 (*SB*) on p53 phosphorylation stimulated by 15d-PGJ_2.** *A,* HUVECs were pretreated with 10 μM MAPK inhibitors as indicated for 1 h and then stimulated with 15d-PGJ_2 for a further 8 h. Cells were harvested and subjected to Western blot analysis using phospho-specific antisera to p53. 15d-PGJ_2-induced p53 was confirmed by probing membranes with total p53 antibody. *B–E,* immunoblots were scanned and quantitated, and p53 phosphorylation at individual sites was normalized to β-actin. *, $p < 0.05$ *versus* 15d-PGJ_2-treated cells. #, $p < 0.002$ *versus* SB203580 +15d-PGJ_2-treated cells. *UT*, untreated.

Effects of JNK and p38 MAPK on p53 Phosphorylation Stimulated by 15d-PGJ_2—MAPKs have been shown to modulate the stability and activity of p53 through affecting the phosphorylation of p53 (26). The potential involvements of JNK and p38 MAPK were examined by Western blot analysis using phosphor-specific antisera to p53. Exposure of cells to 15d-PGJ_2 for 8 h induced the phosphorylation of p53 on Ser-20, Ser-33, Ser-37, and Ser-392 (Fig. 9, *A–D*) and had no effect on Ser-15 and Thr-81 (Fig. 9, *A* and *E*). JNK inhibitor SP600125 pretreatment significantly prevented phosphorylation of p53 on Ser-33 and Ser-392 induced by 15d-PGJ_2 (40 $\pm$ 11 and 35 $\pm$ 6% lower than 15d-PGJ_2-treated cells; Fig. 9, *C* and *D*). SB203580 pretreatment induced p53 phosphorylation on Thr-81 (Fig. 9*E*), suggesting p38 MAPK inhibits a kinase that phosphorylates the Thr-81 of p53. Interestingly, the induction effect of SB203580 on Thr-81 of p53 was partially prevented when cells were co-pretreated with SP600125. In addition, phosphorylation of p53 on Se-20 induced by 15d-PGJ_2 was partially prevented when cells were pretreated with both kinase inhibitors (Fig. 9*B*). Taken together, our findings indicate that 15d-PGJ_2 induces p53 phosphorylated on multiple sites and that JNK and p38 MAPK are involved in this process.

To examine whether 15d-PGJ_2 can also induce p53 phosphorylation in vascular ECs, we stained alkali-treated corneas with aforementioned p53 phosphor-specific antisera after 15d-PGJ_2 treatment for 8 h. However, only anti-p-p53 (Ser-392) antibody in our test condition gives convincing results, showing p53 phosphorylation in nucleus of ECs (Fig. 10*A, green* and *pale blue*). The numbers of p-p53 (S392)-positive nuclei were increased by 15d-PGJ_2 treatment as compared with saline treat-

FIGURE 8. **Inhibitors of p38 MAPK and JNK prevent 15d-PGJ_2-induced apoptosis and the induction of Bax and $p21^{Waf1}$.** *A,* HUVECs were pretreated with SB203580 (*SB*; p38 MAPK inhibitor) or SP600125 (*SP*; JNK inhibitor) for 1 h and then treated with 15d-PGJ_2 for 10 h. Cells were harvested and subjected to Western blot analysis with antibodies as indicated. Representative blots and densitometric analysis from three independent experiments are shown. *B,* untreated (*UT*)- and 15d-PGJ_2-treated cells were also analyzed using the annexin V-FITC apoptosis detection kit according to the *in situ* staining protocol after treatment for 16 h. A representative result of four independent experiments is shown. Double-staining with an annexin V-FITC and the fluorescent dye Hoechst 33342 was employed to visualize the apoptotic cells (*green*) and nuclei (*blue*), respectively. The percentages of apoptotic cells were quantified. *, $p < 0.001$ *versus* 15d-PGJ_2-treated cells. *C,* inhibitors of JNK or p38 MAPK attenuate 15d-PGJ_2-induced vascular EC apoptosis. Animal treatment is described under "Experimental Procedures." After treatment for 24 h, corneas were harvested, and apoptotic endothelial cells (nuclei surrounding annexin V) were quantified as description of Fig. 4. *, $p < 0.05$ *versus* PBS-treated corneas. #, $p < 0.05$ *versus* 15d-PGJ_2-treated corneas.

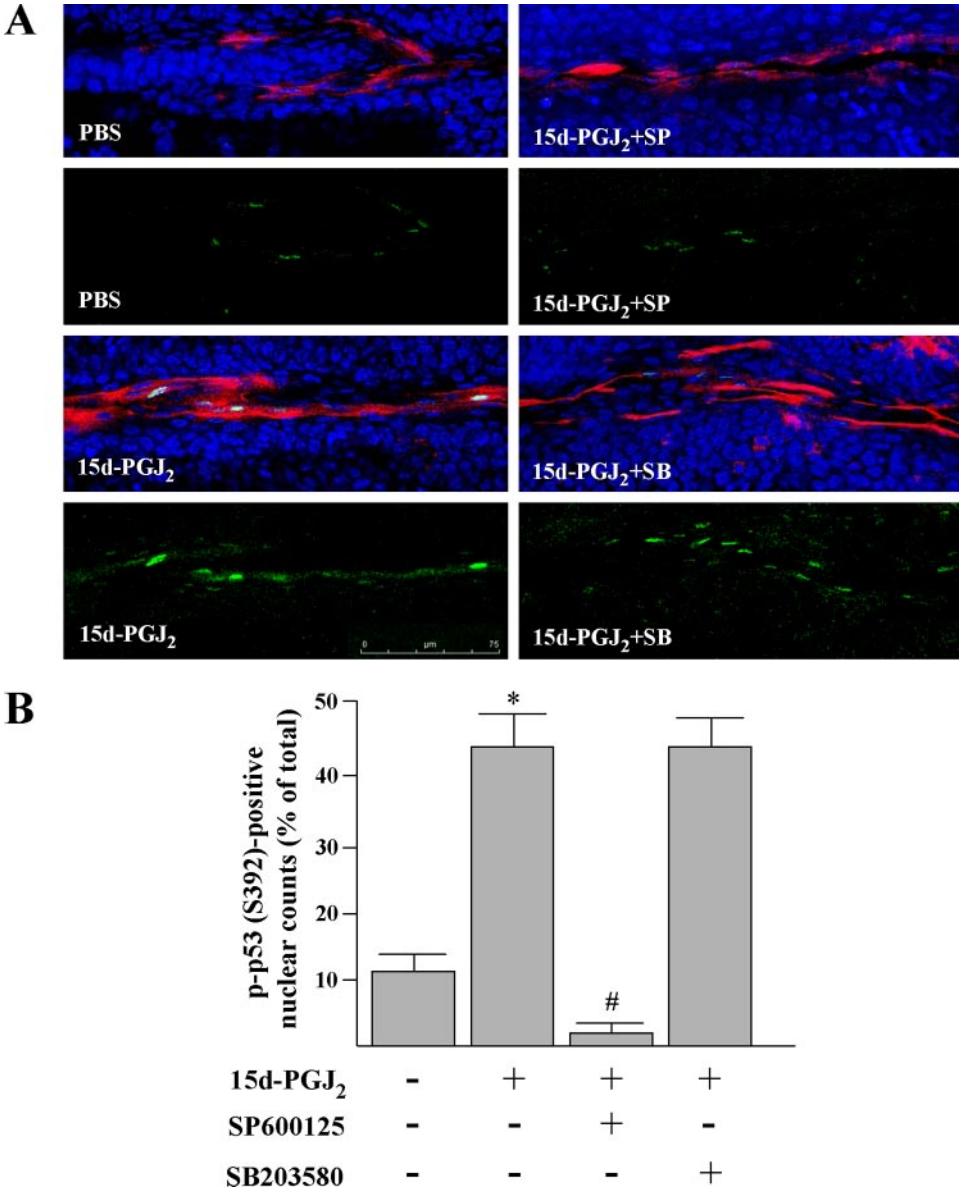

FIGURE 10. **15d-PGJ$_2$ induces a JNK-dependent p53 phosphorylation at Ser-392 in vascular ECs.** Animal treatment is described under "Experimental Procedures." *A,* after treatment for 8 h, corneas were harvested and subjected to immunofluorescent assay for eNOS (*red*) and p-p53 (Ser-392) (*green*). Nuclei were stained by Hoechst 33342 (*blue*). Magnification, ×40. Merged images indicate that 15d-PGJ$_2$ could markedly induce p-p53 (Ser-392) and that the effect was attenuated by the JNK inhibitor but not by the p38 MAPK inhibitor. *B,* percentages of eNOS-positive EC with p-p53-positive nuclei. *, $p < 0.05$ *versus* PBS-treated corneas. #, $p < 0.05$ *versus* 15d-PGJ$_2$-treated corneas.

ment (Fig. 10*B,* 43.2 ± 6% *versus* 11.5 ± 2%). Moreover, the increase of p-p53 (Ser-392)-positive nuclei was prevented by SP600125 co-treatment, indicating a JNK-mediated p53 phosphorylation on Ser-392. In addition, treatment with SP600125 or SB203580 in the absence of 15d-PGJ$_2$ had no effect on the numbers of p-p53 (Ser-392)-positive nuclei (data not shown).

15d-PGJ$_2$ Induces Intracellular ROS Generation That Further Induces p53 Accumulation and MAPKs Phosphorylations—15d-PGJ$_2$ has been shown to induce ROS generation in HUVECs (27). To evaluate the effect of 15d-PGJ$_2$ on intracellular ROS levels in HUVECs, we utilized H_2DCFDA, a dye that generates green fluorescence (DCF fluorescence) when it is oxidized by ROS. Spectrofluorometric assay reveals that HUVECs treated with 15d-PGJ$_2$ for 40 min caused an increase of ROS (Fig. 11*A*). The DCF fluorescence increased 5-fold when cells were treated for 60 min, but this induction was no longer observed at 180 min. Exposure of HUVECs to 1–20 μM 15d-PGJ$_2$ for 60 min increased DCF fluorescence levels in a dose-dependent manner (Fig. 11*B*). Antioxidant, NAC, pretreatment (1–10 mM, 30 min) reduced 15d-PGJ$_2$-induced DCF fluorescence (Fig. 11*C*) and HUVEC apoptosis (Fig. 11*D*) in a dose-dependent manner. The spectrofluorometric assay results were also confirmed under fluorescent microscopy analysis of monolayer cultured cells and revealed that 15d-PGJ$_2$ induced a larger amount of intracellular DCF fluorescence, although the effect was substantially inhibited by 10 mM NAC pretreatment (supplemental Fig. S1*A*). Western blotting results further demonstrated that pretreatment of cells with 1–10 mM NAC significantly reduced 15d-PGJ$_2$-induced apoptotic signaling, including the p53 accumulation and the MAPK phosphorylations, whereas 15d-PGJ$_2$-induced PPARγ protein expression was not abrogated by NAC pretreatment (Fig. 11*E*).

To determine whether 15d-PGJ$_2$ can induce ROS generation *in vivo*, we examined the alkali burned corneas with H_2DCFDA. We found that there is almost no base-line DCF fluorescence in both endothelium and epithelium of mouse cornea (Fig. 12*A*). However, 15d-PGJ$_2$ can induce markedly DCF fluorescence within the vascular ECs of cornea but not in the corneal epithelium. Moreover, NAC pretreatment diminished the 15d-PGJ$_2$-induced DCF fluorescence. These are similar to observations in HUVECs. Cornea pretreated with NAC before 15d-PGJ$_2$ stimulation significantly prevented the vascular EC apoptosis (Fig. 12*B*). Treatment with NAC alone did not induce the apoptosis. In addition, NAC pretreatment can markedly attenuate 15d-PGJ$_2$-induced phosphorylations of JNK, p38 MAPK, and p53 at serine 392 (supplemental Fig. S1, *B–D*). Collectively, these data demonstrate that the induced ROS is an early pro-apoptotic activator for EC apoptosis both *in vitro* and *in vivo*.

15d-PGJ$_2$ Partially Suppresses NF-κB Activity—We also examined the involvement of NF-κB activity in 15d-PGJ$_2$-in-

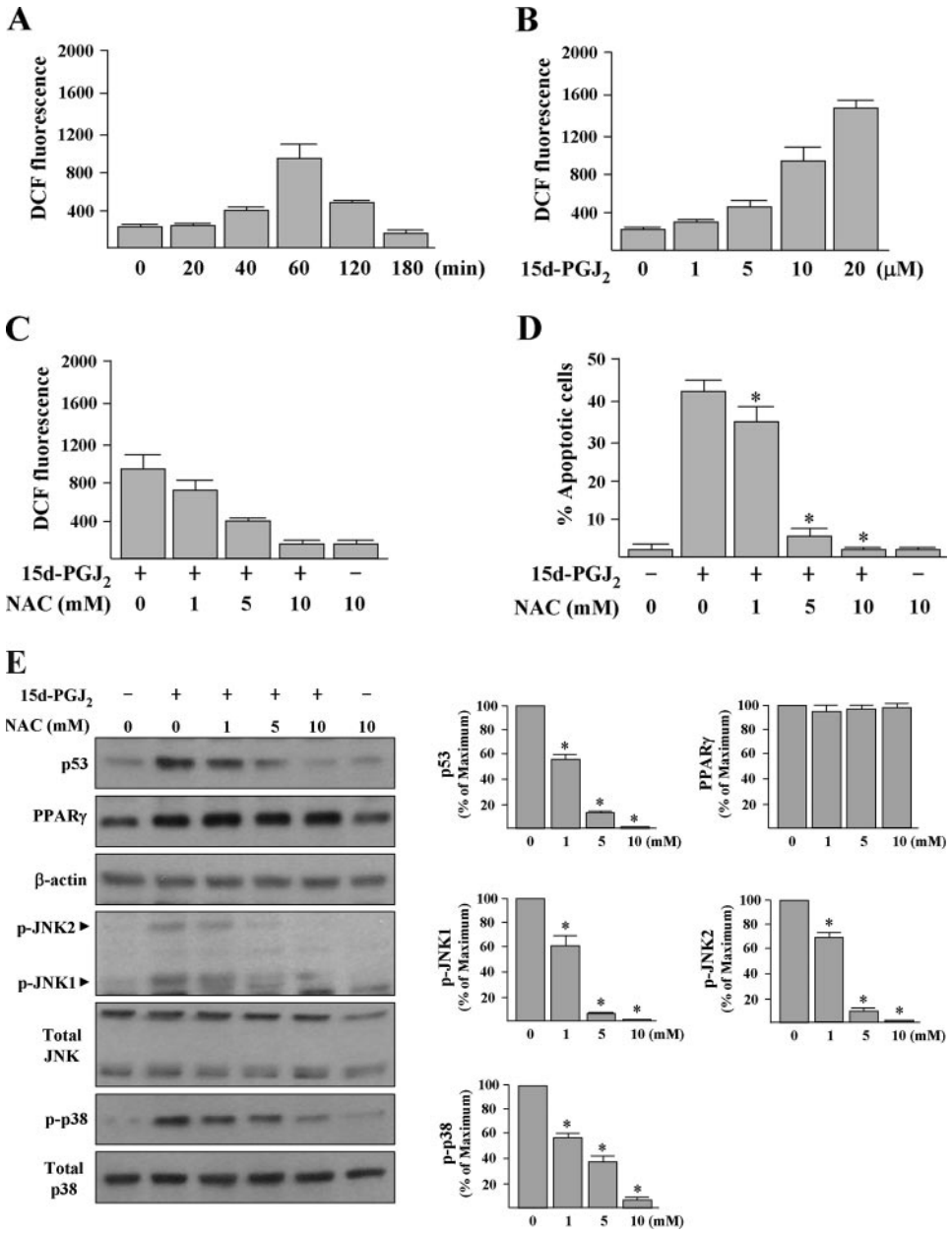

FIGURE 11. **15d-PGJ$_2$-induced HUVEC apoptosis depends on ROS generation.** *A* and *B*, 15d-PGJ$_2$ time- and dose-dependently induces ROS production. HUVECs were treated with 10 μM 15d-PGJ$_2$ for the indicated time periods or various concentrations of 15d-PGJ$_2$ for 1 h. ROS production was expressed as DCF fluorescence intensity per 1.2×10^4 cells and quantified by spectrofluorometry. *C* and *D*, antioxidant NAC prevents ROS formation and HUVEC apoptosis induced by 15d-PGJ$_2$. HUVECs were pretreated or not with various concentrations of NAC as indicated for 30 min prior to treatment of 10 μM 15d-PGJ$_2$. DCF fluorescence was examined after treatment of 15d-PGJ2 for 1 h. Apoptosis was examined after treatment of 15d-PGJ2 for 16 h by counting the annexin V-positive cells. *, $p < 0.05$ *versus* 15d-PGJ$_2$-treated cells. *E*, HUVECs were treated with various concentrations of NAC as indicated for 30 min prior to incubation with 15d-PGJ$_2$ for additional 8 h. Cellular proteins were extracted for Western blot analysis. Representative blots and densitometric analysis with S.D. are shown. *, $p < 0.001$ *versus* 15d-PGJ$_2$-treated cells.

duced apoptosis, because it is known that NF-κB belongs to a redox-sensitive transcription factor and interferes with the induction of apoptosis (28). First, we investigated the potential influence of 15d-PGJ$_2$ on the phosphorylations of NF-κB and IκB-α. Western blot analysis revealed that there were no markedly alterations on the phosphorylations of IκB-α and p65 after treatment with 15d-PGJ$_2$ at all time periods studied. In addition, NAC did not alter the levels of phosphorylations of IκB-α and NF-κB p65 subunit (Fig. 13*A*). We further assayed the levels of the active form of NF-κB in 15d-PGJ$_2$-stimulated cells by a modified electromobility shift assay. We found that the DNA binding activity of NF-κB was significantly repressed by 20–30% after 15d-PGJ2 treatment for 2–8 h (Fig. 13*B*). The 15d-PGJ$_2$-mediated inhibitory effect was reversed by NAC pretreatment, implying that 15d-PGJ$_2$-induced ROS is responsible for this inhibition. Moreover, HUVECs pretreated with the nonlethal dose of NF-κB activation inhibitor (5 μM 6-amino-4-(4-phenoxyphenylethylamino)quinazoline) or NF-κB nuclear translocation inhibitor (10 μM SN50) significantly enhanced the 15d-PGJ$_2$-induced apoptosis from 42 ± 4% to 56 ± 4 and 50 ± 5%, respectively (Fig. 13*C*), suggesting that NF-κB basal activity can restrict the 15d-PGJ$_2$-induced apoptosis. To further investigate the distribution of p65 *in vivo*, alkali burned mouse cornea was treated with 15d-PGJ$_2$ for 8 h. Immunofluorescent assay showed that most of p65 was localized in the cytoplasm but rarely in the nuclei in PBS-treated cornea, whereas the distribution was not altered by 15d-PGJ$_2$ (Fig. 13*D*). This suggests that 15dPGJ$_2$ effects on vascular ECs of cornea are independent of NF-κB nuclear translocation.

DISCUSSION

Presently, we have a limited understanding about the apoptosis-inducing mechanism of 15d-PGJ$_2$ in ECs. In culture, in addition to apoptosis, 15d-PGJ$_2$ has been shown to dose-dependently inhibit several functions of ECs related to angiogenesis, such as proliferation, morphogenesis, and migration (2, 3, 6). However, the *in vivo* mechanisms of anti-angiogenesis by 15d-PGJ$_2$ remain unclear. Previous observations of the inhibitory effect from mixing VEGF and 15d-PGJ$_2$ did not address this (3). In this study, EC apoptosis was identified in a mouse cornea neovascularization model. Based on the massive apoptosis of vascular ECs, it is plausible to propose apoptosis as the major mechanism of the pharmacological effect of 15d-PGJ$_2$ *in vivo*.

It has been found that 15d-PGJ$_2$ induces neuronal apoptosis through a p53-dependent mechanism (17). The increase of p53 protein level by 15d-PGJ$_2$ treatment through an unknown

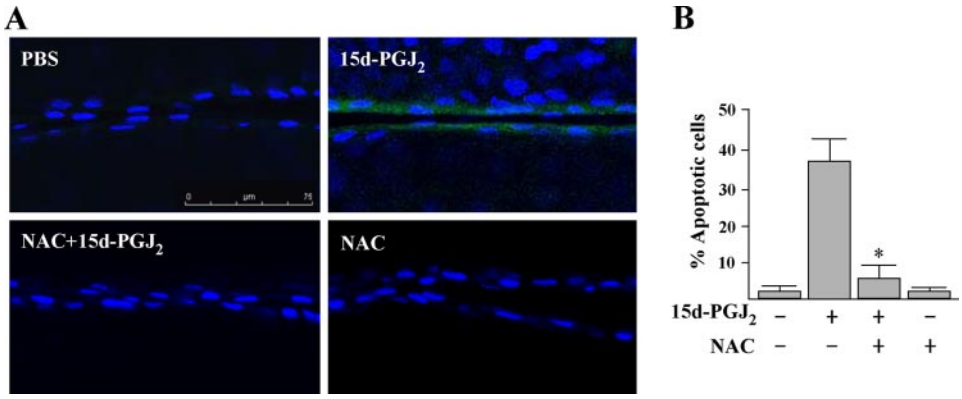

FIGURE 12. *A*, 15d-PGJ_2 induces ROS generation in vascular ECs. Mice bearing chemical burn-induced corneal neovascularization were exposed to 10 mM NAC for 30 min before treatment with 15d-PGJ_2 for a further 1 h. Detection of ROS by H_2DCFDA in corneal vascular EC is described under "Experimental Procedures." *B*, antioxidant NAC attenuates 15d-PGJ_2-induced vascular EC apoptosis. Animal treatment is as described above. After treatment for 24 h, corneas were harvested and apoptotic ECs (nuclei surrounding annexin V) were quantified as description of Fig. 4. *, $p < 0.05$ *versus* 15d-PGJ_2-treated corneas.

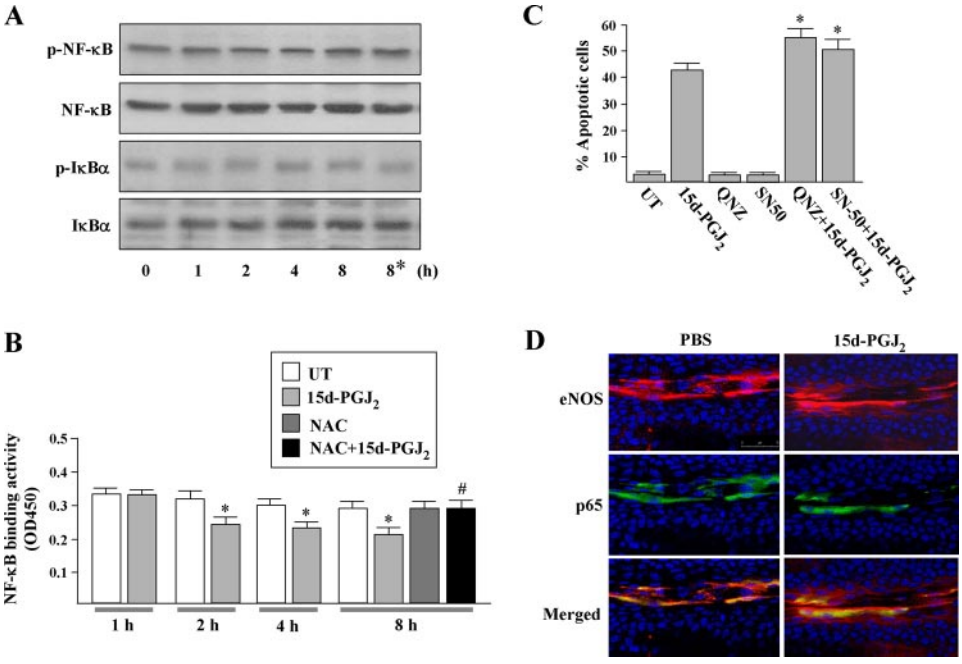

FIGURE 13. **Analyses of NF-κB properties in ECs stimulated by 15d-PGJ_2.** *A*, HUVECs were treated with 10 μM 15d-PGJ_2 for the indicated time periods. Cells were harvested and subjected to Western blot analysis using phospho-specific antisera to NF-κB or IκBα and then probing membranes with total NF-κB or IκBα antibody. *Asterisk* indicates cells were treated with 10 mM NAC for 30 min prior to treatment with15d-PGJ_2. Shown are blots representative of at least three independent experiments. *B*, NF-κB activity. Nuclear extracts from 5×10^5 HUVECs were measured for the NF-κB DNA binding activity by ELISA ($n = 4$). *, $p < 0.05$ *versus* untreated (*UT*) cells. #, $p < 0.005$ *versus* 15d-PGJ_2-treated cells. *C*, HUVECs were treated with inhibitors of NF-κB (5 μM; 6-amino-4-(4-phenoxyphenylethylamino)quinazoline (*QNZ*) or 10 μM SN50, 1 h) before exposure to 15d-PGJ_2 for a further 16 h, and then apoptosis was examined by counting the annexin V-positive cells. *, $p < 0.05$ *versus* 15d-PGJ_2-treated cells. *D*, 15d-PGJ_2 effect on the cellular distribution of NF-κB p65 subunit in vascular ECs. Mouse corneas were subjected to alkali trauma and eyes were treated 3 days later with either 20 μl of PBS or 20 μM 15d-PGJ_2. After treatment for 8 h, corneas were harvested and subjected to immunofluorescence for eNOS (*red*) and p65 (*green*). Nuclei were stained by Hoechst 33342 (*blue*). Magnification, ×40. *Bar*, 75 μm.

mechanism has been reported in immortalized endothelial cells (6), human articular chondrocytes (18), and non-small cell lung cancer cell lines (29), although this effect is not linked to apoptosis in these observations. These prompted us to investigate the involvement of p53 in 15d-PGJ_2-induced EC apoptosis. In this study, several lines of evidence indicate that the induction of HUVEC apoptosis by 15d-PGJ_2 is mediated by p53. The concentrations of 15d-PGJ_2 required to increase p53 protein expression are the same as to induce apoptosis. Pretreatment with siRNA targeting p53 not only checked the p53 increase but also significantly prevented 15d-PGJ_2-induced apoptosis of HUVECs and corneal vascular ECs. Therefore, our results further highlight the importance of p53 in apoptotic cell death induced by 15d-PGJ_2.

NF-κB, a crucial transcriptional activator of multiple anti-apoptotic genes is considered important for resistance to many apoptotic stimuli (30). It has been reported that 15d-PGJ_2 at high concentrations can suppress NF-κB transcriptional activity by induction of IκB-α kinase degradation to promote tumor necrosis factor-α-mediated HUVEC cell death (4). Our results revealed that 15d-PGJ_2 could partially inhibit NF-κB DNA binding activity. In particular, 15d-PGJ_2-induced HUVEC apoptosis was enhanced by pharmacological inhibitions of NF-κB activation or nuclear translocation. These suggest that NF-κB signaling can at least partially protect ECs from 15d-PGJ_2-induced apoptosis. Therefore, it is also possible that 15d-PGJ_2 acts through dual effects, inhibition of NFκB and activation of p53, to induce prominent EC apoptosis.

PPARγ agonists have shown considerable pre-clinical efficacy by their anti-angiogenic effect (31). Although 15d-PGJ_2 is the natural ligand of PPARγ, there are conflicting reports about 15d-PGJ_2 in terms of PPARγ dependence (2, 7). In this study, the induction of the PPARγ pathway by 15d-PGJ_2 is evident from the induction of PPARγ gene expression via a known autoregulation pathway. However, the PPARγ-specific inhibitors failed to prevent 15d-PGJ_2-induced apoptosis as well as the induction of p53, indicating a PPARγ-independent pathway for 15d-PGJ_2-induced HUVEC apoptosis. Interestingly, it has been reported that 15d-PGJ_2 induces apoptosis of human articular chondrocytes in a PPARγ-dependent manner (18), whereas the induction of human hepatic myofibroblast apoptosis is independent of PPARγ (32). These suggest the role of PPARγ in 15d-PGJ_2-mediated apoptosis may be cell type-dependent.

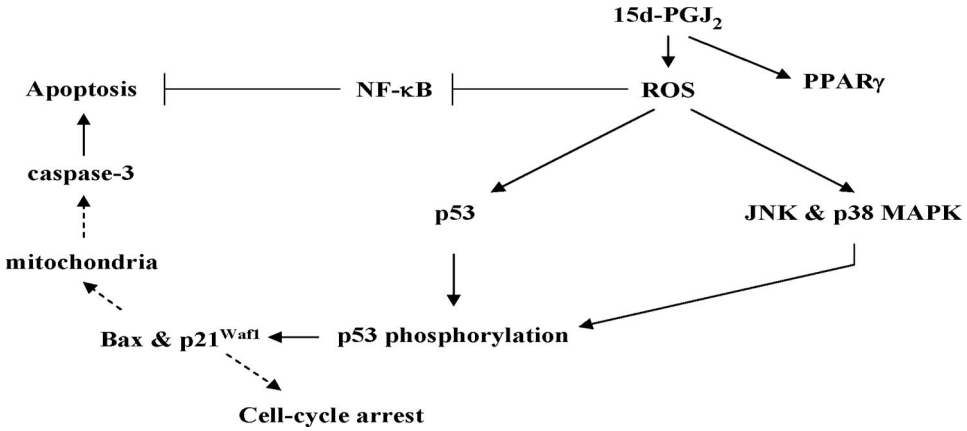

FIGURE 14. **Schematic summary of 15d-PGJ$_2$-mediated apoptotic pathway in ECs.** In this scheme, 15d-PGJ$_2$ induces ROS generation, leading to p53 accumulation, activation of both JNK and p38 MAPK, and partial prevention of NF-κB activity. 15d-PGJ$_2$ also induces PPARγ overexpression by ROS-independent mechanism. JNK and p38 MAPK play a crucial role in induction of p53 phosphorylation and activation that leads to increased Bax and p21^{Waf1} expression. The increased Bax may cause mitochondria-induced cleavage of procaspases-3 to cause apoptosis. The linkages inferred, but not directly tested, are indicated with *dashed arrows*.

In this study, the increase of p53 levels seems to be mediated by stabilization rather than synthesis. The p53 mRNA level remains unchanged by 15d-PGJ$_2$ exposure. On the other hand, the stability of p53 protein is increased. p53 is metabolized through ubiquitin-mediated proteasome degradation. A previous study reported that the electrophilic feature of 15d-PGJ$_2$ is involved in the inhibition of proteasome activities, leading to p53 protein accumulation in SH-SY5Y human neuroblastoma cells (33). In addition, the regulation of p53 stability is linked to the modification of p53 by phosphorylation at various sites (26). To take DNA damage by ultraviolet radiation as an example, p53 is phosphorylated on serines 15, 20, and 37 deterring the association between p53 and the E3 ubiquitin ligase Mdm2 and preventing p53 ubiquitinization (34, 35). Our results revealed that certain p53 phosphorylations, including serine 20 of p53, were found to be mediated by both JNK and p38 MAPK. However, in the system we studied, p53 is not stabilized by JNK and p38 MAPK, because inhibitors of either kinase failed to decrease p53 levels. The exact mechanisms for p53 stabilization in 15d-PGJ$_2$-stimulated HUVECs remain to be determined, especially regarding the inhibition of the degradation function of the proteasome.

Previous studies have been shown that 15d-PGJ$_2$ elicits p38 MAPK activation that plays an essential role in induction of apoptosis of human articular chondrocytes (18) and a human pancreatic cancer cell line (19). However, the target for p38 MAPK to trigger cells to enter apoptosis remains unclear. In this study, we demonstrate for the first time a link between not only p38 MAPK but also JNK and p53 as depicted in Fig. 14. First, the protective effect of the JNK inhibitor or the p38 MAPK inhibitor on 15d-PGJ$_2$-induced HUVEC apoptosis is similar to p53 siRNA pretreatment, suggesting that JNK and p38 MAPK may trigger nonredundant signaling to modulate p53-induced apoptosis. Second, the p53 phosphorylation pattern induced by 15d-PGJ$_2$ was altered when HUVECs were pretreated with either JNK inhibitor or p38 MAPK inhibitor, suggesting that JNK and p38 MAPK could modulate p53 transcriptional activity. The suggestion is further supported by the results that inhibitors also can attenuate the expression of Bax and p21^{Waf1}.

p53 activation by stressful stimuli involves functional interaction with MAPKs that phosphorylate p53 at various sites, mainly located at the NH_2 terminus transactivation domain and a proline-rich domain (26). Phosphorylation of p53 at Ser-33 (36) or Ser-392 (37, 38) or Thr-81 (39) is essential for p53 transcriptional activity in genotoxic drug-induced apoptosis. In this study, we found that p53 phosphorylation at various sites is modulated by 15d-PGJ$_2$. The mechanism of change of individual phosphorylation sites remains elusive. On the other hand, JNK and p38 MAPK seem to participate in the phosphorylations of p53 at different sites as evident from observations that JNK inhibitor prevents p53 phosphorylation on Ser-33 and Ser-392, whereas p38 MAPK inhibitor increases p53 phosphorylation on Thr-81 under 15d-PGJ$_2$ stimulation. JNK reportedly phosphorylates p53 at Thr-81 in response to DNA damage in 293T cells (40). It has been shown that inhibition of p38 MAPK activation after UV irradiation decreases p53 phosphorylation at Ser-33, Ser-37, and Ser-15 accompanying markedly reduced UV-induced apoptosis (41). These observations suggest p38 MAPK and JNK are capable of mediating p53 phosphorylation induced by 15d-PGJ$_2$. However, although JNK and p38 MAPK activities are essential for p53-mediated apoptosis, we cannot conclude that direct phosphorylation at these sites is the sole mechanism by which JNK and p38 MAPK mediated the effect of 15d-PGJ$_2$.

It has been demonstrated that the exogenous 15d-PGJ$_2$ can directly interact with mitochondria leading to the generation of ROS in ECs (27). Using H_2DCFDA, we confirmed the presence of ROS in 15d-PGJ$_2$-treated HUVECs and vascular ECs of cornea, which precedes 15d-PGJ$_2$-induced apoptotic signaling, including p53 accumulation, MAPK phosphorylations, and inhibition of NF-κB activity (Fig. 14). It may be important to our findings that 15d-PGJ$_2$ reportedly can covalently modify the p50 subunit by alkylation of a cysteine located at the DNA-binding domain of p50 to impair NF-κB transcriptional activity (15, 42). On the other hand, our results also shown that NAC pretreatment was able to abolish these 15d-PGJ2-induced apoptotic signalings. NAC, a precursor molecule for glutathione (GSH) synthesis, is usually used to monitor the effect of GSH supplementation *in vitro*. In particular, GSH is an important antioxidant that protects cells from oxidative damage by ROS, although it has been found that 15d-PGJ$_2$ induces cell death by decrease of the intracellular level of GSH (43–45). Therefore, it is possible that the GSH depletion may be an early molecular event, leading to triggering of 15d-PGJ$_2$-induced oxidative stress responses in HUVECs and in vascular ECs of cornea.

In conclusion, our study demonstrated that 15d-PGJ$_2$ induces EC apoptosis through the signaling of JNK and p38

MAPK-mediated p53 activation both in *in vitro* and *in vivo*. The ability to induce vascular EC apoptosis *in vivo* suggests that 15d-PGJ_2 cannot only prevent the formation of new vessels but also eliminate existing abnormal vessels. Our data provide the pharmacological basis for developing 15d-PGJ_2 into clinically important therapeutics.

REFERENCES

1. Zhang, S. X., and Ma, J. X. (2006) *Prog. Retin Eye Res.* **26,** 1–37
2. Bishop-Bailey, D., and Hla, T. (1999) *J. Biol. Chem.* **274,** 17042–17048
3. Xin, X., Yang, S., Kowalski, J., and Gerritsen, M. E. (1999) *J. Biol. Chem.* **274,** 9116–9121
4. Zernecke, A., Erl, W., Fraemohs, L., Lietz, M., and Weber, C. (2003) *FASEB J.* **17,** 1099–1101
5. Vosseler, C. A., Erl, W., and Weber, P. C. (2003) *Biochem. Biophys. Res. Commun.* **307,** 322–326
6. Dong, Y. G., Chen, D. D., He, J. G., and Guan, Y. Y. (2004) *Acta Pharmacol. Sin.* **25,** 47–53
7. Erl, W., Weber, C., Zernecke, A., Neuzil, J., Vosseler, C. A., Kim, H. J., and Weber, P. C. (2004) *Eur. J. Immunol.* **34,** 241–250
8. Murakami, M., Nakatani, Y., Kuwata, H., and Kudo, I. (2000) *Biochim. Biophys. Acta* **1488,** 159–166
9. Fukushima, M. (1992) *Fatty Acids* **47,** 1–12
10. Forman, B. M., Tontonoz, P., Chen, J., Brun, R. P., Spiegelman, B. M., and Evans, R. M. (1995) *Cell* **83,** 803–812
11. Kliewer, S. A., Lenhard, J. M., Willson, T. M., Patel, I., Morris, D. C., and Lehmann, J. M. (1995) *Cell* **83,** 813–819
12. Rizzo, G., and Fiorucci, S. (2006) *Curr. Opin. Pharmacol.* **6,** 421–427
13. Duan, S. Z., Usher, M. G., and Mortensen, R. M. (2008) *Circ. Res.* **102,** 283–294
14. Uchida, K., and Shibata, T. (2007) *Chem. Res. Toxicol.* **21,** 138–144
15. Straus, D. S., Pascual, G., Li, M., Welch, J. S., Ricote, M., Hsiang, C. H., Sengchanthalangsy, L. L., Ghosh, G., and Glass, C. K. (2000) *Proc. Natl. Acad. Sci. U. S. A.* **97,** 4844–4849
16. Ho, T. C., Chen, S. L., Yang, Y. C., Liao, C. L., Cheng, H. C., and Tsao, Y. P. (2007) *Cardiovasc. Res.* **76,** 213–223
17. Kondo, M., Shibata, T., Kumagai, T., Osawa, T., Shibata, N., Kobayashi, M., Sasaki, S., Iwata, M., Noguchi, N., and Uchida, K. (2002) *Proc. Natl. Acad. Sci. U. S. A.* **99,** 7367–7372
18. Shan, Z. Z., Masuko-Hongo, K., Dai, S. M., Nakamura, H., Kato, T., and Nishioka, K. (2004) *J. Biol. Chem.* **279,** 37939–53790
19. Hashimoto, K., Farrow, B. J., and Evers, B. M. (2004) *Pancreas* **28,** 153–159
20. Teodoro, J. G., Parker, A. E., Zhu, X., and Green, M. R. (2006) *Science* **313,** 968–971
21. Pasquier, E., Carré, M., Pourroy, B., Camoin, L., Rebaï, O., Briand, C., and Braguer, D. (2004) *Mol. Cancer Ther.* **3,** 1301–1310
22. Xia, Z., Dickens, M., Raingeaud, J., Davis, R. J., and Greenberg, M. E. (1995) *Science* **270,** 1326–3131
23. Chang, L., and Karin, M. (2001) *Nature* **410,** 37–40
24. Chen, N. G., and Han, X. (2001) *Biochem. Biophys. Res. Commun.* **282,** 717–722
25. Tsao, Y. P., Ho, T. C., Chen, S. L., and Cheng, H. C. (2006) *Life Sci.* **79,** 545–550
26. Wu, G. S. (2004) *Cancer Biol. Ther.* **3,** 156–161
27. Landar, A., Zmijewski, J. W., Dickinson, D. A., Le Goffe, C., Johnson, M. S., Milne, G. L., Zanoni, G., Vidari, G., Morrow, J. D., and Darley-Usmar, V. M. (2006) *Am. J. Physiol.* **290,** H1777–H1787
28. Bubici, C., Papa, S., Dean, K., and Franzoso, G. (2006) *Oncogene* **25,** 6731–6748
29. Fulzele, S. V., Chatterjee, A., Shaik, M. S., Jackson, T., Ichite, N., and Singh, M. (2007) *Anticancer Drugs* **18,** 65–78
30. Shishodia, S., and Aggarwal, B. B. (2002) *J. Biochem. Mol. Biol.* **35,** 28–40
31. Giaginis, C., Margeli, A., and Theocharis, S. (2007) *Exp. Opin. Investig. Drugs* **16,** 1561–1572
32. Li, L., Tao, J., Davaille, J., Feral, C., Mallat, A., Rieusset, J., Vidal, H., and Lotersztajn, S. (2001) *J. Biol. Chem.* **276,** 38152–38158
33. Shibata, T., Yamada, T., Kondo, M., Tanahashi, N., Tanaka, K., Nakamura, H., Masutani, H., Yodoi, J., and Uchida, K. (2003) *Biochemistry* **42,** 13960–13968
34. Bean, L. J., and Stark, G. R. (2001) *Oncogene* **20,** 1076–1084
35. Chehab, N. H., Malikzay, A., Stavridi, E. S., and Halazonetis, T. D. (1999) *Proc. Natl. Acad. Sci. U. S. A.* **96,** 13777–13782
36. Sanchez-Prieto, R., Rojas, J. M., Taya, Y., and Gutkind, J. S. (2000) *Cancer Res.* **60,** 2464–2472
37. Holownia, A., Mroz, R. M., Kozlowski, M., Chyczewska, E., Laudanski, J., Chyczewski, L., and Braszko, J. J. (2003) *Neoplasma* (*Bratisl.*) **50,** 266–271
38. Harmand, P. O., Duval, R., Liagre, B., Jayat-Vignoles, C., Beneytout, J. L., Delage, C., and Simon, A. (2003) *Int. J. Oncol.* **23,** 105–112
39. Zacchi, P., Gostissa, M., Uchida, T., Salvagno, C., Avolio, F., Volinia, S., Ronai, Z., Blandino, G., Schneider, C., and Del Sal, G. (2002) *Nature* **419,** 853–857
40. Buschmann, T., Potapova, O., Bar-Shira, A., Ivanov, V. N., Fuchs, S. Y., Henderson, S., Fried, V. A., Minamoto, T., Alarcon-Vargas, D., Pincus, M. R., Gaarde, W. A., Holbrook, N. J., Shiloh, Y., and Ronai, Z. (2001) *Mol. Cell. Biol.* **21,** 2743–2754
41. Bulavin, D. V., Saito, S., Hollander, M. C., Sakaguchi, K., Anderson, C. W., Appella, E., and Fornace, A. J., Jr. (1999) *EMBO J.* **18,** 6845–6854
42. Cernuda-Morollón, E., Pineda-Molina, E., Cañada, F. J., and Pérez-Sala, D. (2001) *J. Biol. Chem.* **276,** 35530–35536
43. Kim, H. S., Lee, J. H., and Kim, I. K. (1996) *Prostaglandins* **51,** 413–425
44. Ray, D. M., Akbiyik, F., and Phipps, R. P. (2006) *J. Immunol.* **177,** 5068–5076
45. Figarella, K., Uzcategui, N. L., Beck, A., Schoenfeld, C., Kubata, B. K., Lang, F., and Duszenko, M. (2006) *Cell Death Differ.* **13,** 1802–1814